Using Petroleum and Biomass-Derived Fuels in Duel-fuel Diesel Engines

Suresh K. Aggarwal and Xiao Fu

Abstract There is worldwide interest in developing renewable energy sources in a sustainable manner. Syngas and biogas offer significant potential in this context, as these fuels offer great flexibility with regard to their production and utilization. This chapter provides an overview of research dealing with the combustion and emission characteristics of these fuels, both as stand-alone fuels or by blending with petroleum fuels. Conversion methods for producing these fuels from different biomass sources are also briefly reviewed. While the syngas composition can vary widely, it generally has lower heating value, lower density, higher mass diffusivity, higher flame speeds, and wider flammability limits compared to hydrocarbon fuels. Moreover, its combustion leads to almost zero soot emission, although NO_x emission may be a concern depending upon its composition and operating temperatures. Similarly, biogas has lower heating value compared to hydrocarbon fuels, and its ignition and combustion characteristics can vary noticeably depending upon its composition. While there have been few studies focusing directly on biogas combustion, there is extensive literature on methane combustion, including ignition, extinction, flammability limits, flame speeds, cellular instabilities, and emissions. Fundamental combustion aspects requiring further research include cellular instabilities, flame stabilization and blowout behavior, turbulent flames, and emission characteristics. Such efforts would lead to the development of optimized systems for producing these fuels and provide guidelines for optimizing their composition for a given set of operating conditions. The use of syngas and biogas in dual-fuel diesel engines has been a subject of numerous experimental and computational studies. A general observation is that the engine performance and emission characteristics are significantly modified by the presence of gaseous fuel. While the heat release in a diesel engine generally occurs through a hybrid combustion mode,

S.K. Aggarwal (✉)
Flow and Combustion Laboratory, Department of Mechanical Engineering,
University of Illinois at Chicago, Chicago, IL 60607, USA
e-mail: ska@uic.edu

X. Fu
Flow and Combustion Simulation Laboratory, Department of Mechanical
and Industrial Engineering, University of Illinois at Chicago, Chicago, IL 60607, USA

A.K. Agarwal et al. (eds.), *Novel Combustion Concepts for Sustainable Energy Development*, DOI 10.1007/978-81-322-2211-8_11

involving rich premixed combustion and diffusion combustion, that in a dual-fuel engine also involves a lean combustion mode with a propagating flame. The dual-fuel operation at high-load conditions can provide significant reduction in soot and CO soot emissions, while maintaining the engine efficiency, provided the injection characteristics including the amount of pilot fuel can be optimized. However, the NO_x emission may increase, requiring a suitable strategy for lowering the temperatures. The dual-fuel strategy may be less effective at low load, resulting in lower thermal efficiency and higher UHC and CO emissions. Future work should be directed at optimizing the various parameters, such as injection timing, amount of pilot fuel injected, EGR, and multiple injections.

Keywords Syngas · Biogas · Combustion and emissions · Dual-fuel engines

1 Introduction

There is a worldwide interest in developing renewable energy sources in a sustainable manner. This is motivated by concerns about depleting fossil energy sources, climate change due to greenhouse gas emissions, and growing energy needs due to emerging economies and population growth. The climate change concerns are illustrated in Fig. 1, which provides an historic perspective on the concentrations of three most significant greenhouse gases and their contributions to the increase in radiative forcing (W/m^2). As indicated, the CO_2 concentration in atmosphere has increased by 31 %, accounting for 1.46 W/m^2 change in radiative forcing since 1800. Clearly, a sustainable and carbon-neutral energy future will require a significant broadening of our energy portfolio and reducing reliance on non-renewable sources. The non-food and regional fuel sources, especially biomass, can potentially play a major role in this regard. Biomass represents one of the primary energy resources in the world after coal and oil, particularly in developing countries (Hall et al. 1991). It refers to a broad variety of feedstock ranging from agricultural waste, such as straw, bagasse, rice husks, olive pits, and nuts, to energy crops, such as, *miscanthus* and *sorghum* (Werther et al. 2000). It also includes algae, forestry waste, such as wood chips, bark, and thinnings, and other solid wastes including sewage sludge, as well as municipal solid waste. The use of biomass would not only reduce our dependence on fossil energy sources, but also provide energy in a sustainable and carbon neutral manner.

While a variety of fuels can be produced from biomass, syngas and biogas seem to offer the most potential with respect to flexibility in their production and utilization. Syngas can be produced using a variety of feedstock and conversion processes, particularly gasification, while biogas is generally produced by anaerobic digestion of biodegradable materials in an oxygen-free environment (Wikipedia 2014). Syngas mainly consists of H_2 and CO with varying amounts of CH_4 and CO_2, with the main constituents of biogas include CH_4, CO_2, and N_2 along with small traces of H_2O, O_2, H_2, and hydrogen sulfide. Both of these fuels represent a

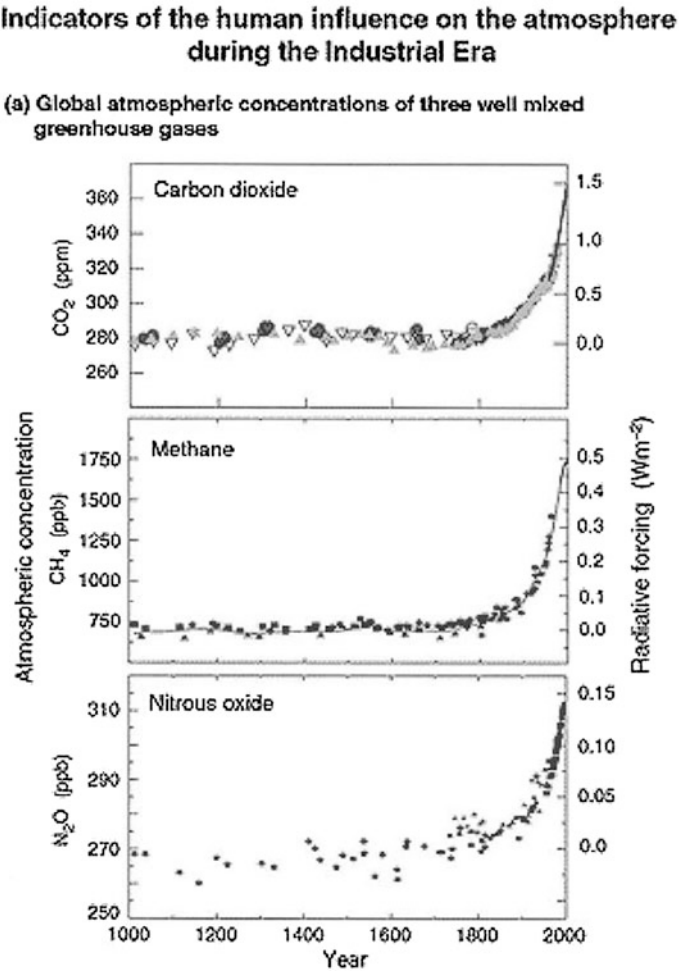

Fig. 1 Global atmospheric concentrations of three most important greenhouse gases

cleaner and renewable energy source and offer great flexibility in their utilization for transportation and power generation. This chapter provides an overview of research dealing with the combustion and emissions of these fuels, both as stand-alone fuel or by blending with petroleum fuels. Clearly, there is a vast body of literature on the fundamental and applied research concerning the production and utilization of these fuels. However, the scope of this chapter is limited to fundamental work concerning their ignition behavior, laminar flame burning these fuels, and the use of these fuels in dual-fuel diesel engines.

The chapter is organized in the following manner. The next section provides a brief summary of processes for converting biomass to more useful fuels, followed by an overview of fundamental studies on the combustion and emission

characteristics of syngas and biogas fuels. Studies dealing with the use of syngas and biogas in dual-fueled diesel engines are discussed in Sect. 4, and a summary is provided in the last section.

2 Conversion Methods

Biomass can be converted to more valuable energy forms through a number of processes including mechanical or physical, biological, and thermochemical. A review of various conversion processes and major products (fuels) produced from ligocellulogic biomass is provided by Gill et al. (2011). An example of mechanical process is the extraction of oil from the seeds of biomass crops, such as oilseed rape and groundnuts. This oil can be used directly for the production of energy or processed using esterification to produce biodiesel. Examples of biological methods include the production of biogas from anaerobic digestion or the breakdown of biodegradable material, such as municipal waste and plant material, through microorganisms (Lin and Tanaka 2006), and the fermentation of sugar to produce ethanol and other biofuels.

Thermochemical methods, which include direct biomass combustion, pyrolysis and gasification, have been extensively investigated for the conversion of biomass to a variety of products, including thermal energy, fuels, and chemicals. Direct biomass combustion has traditionally been used to supply heat and power in the process industry. Systems utilizing direct combustion of agricultural waste include kilns and boilers for generating steam used for various industrial applications including electricity production. As discussed by Werther et al. (2000) in their review paper, the typical sequence of events through which a lump of solid fuel undergoes during combustion includes heating up, drying, devolatilization, ignition and combustion of volatiles, and finally the combustion of char. In general, the route involving direct combustion of biomass for electricity generation has low overall efficiency and emits significant pollutants (Caputo et al. 2005). For the details of these processes, and the discussion of many operational and environmental challenges, the reader is referred to their review paper.

Pyrolysis refers to the thermal decomposition of biomass in the absence of oxygen. Depending on the process variables, such as the reactor temperature and residence time, it yields various amounts of gaseous, liquid, and solid products of varying compositions. Conventional pyrolysis, which has been utilized for thousands of years, involves lower temperatures and longer residence times with the principal product being the solid char. In contrast, fast pyrolysis involves high temperatures (≈500 °C) and short residence times (≈2 s), with the main product being a dark brown liquid or bio-oil along with other gaseous, liquid, and solid products, including char. This process is much more commonly used at present compared to conventional pyrolysis. The bio-oil consists of a complex mixture of oxygenated hydrocarbons with varying but appreciable amount of water from both the original moisture and reaction product. Proximate analysis of the bio-oil gives a

chemical formula of $CH_{1.9}O_{0.7}$. The typical heating value of bio-oil is about 17 MJ/kg, which is about 40–45 % of that of hydrocarbon fuels. The physical properties of bio-oils are discussed by Czernik and Bridgwater (2004), while Bridgwater (2012) and Mohan et al. (2006) provide reviews on fast pyrolysis and the properties of bio-oils generated from this process. Bio-oil can be utilized in several different ways to produce energy, fuels, and chemicals. It has been used directly as fuels in stationary applications, especially for electricity generation. A more sustainable and value-added approach is based on a bio-refinery concept, similar to a petroleum refinery, for producing energy, conventional fuels, such as syngas and Fischer-Tropsch (FT) fuels, and chemicals. This concept is particularly attractive for biomass because of its chemical heterogeneity and regional variability.

Biomass gasification involves pyrolysis and partial oxidation in a well-controlled oxidizing environment. It is deemed as the most promising technology for producing renewable and carbon-free energy, as it provides great flexibility with regard to feedstock and the fuels produced. In recent years, numerous studies have reported on the different types of reactors used in gasification, and the various gaseous and liquid fuels produced. Wang et al. (2008b) and Gill et al. (2011) provide reviews of these studies. In general, the gasification process converts low-value biomass to a gaseous mixture containing syngas and varying amounts of CH_4 and CO_2. It can also produce hydrocarbons by using lower operating temperatures. The syngas composition, or the relative amounts of CO and H_2 in the syngas, can be varied by using air and steam as the gasification agent (Rapagna et al. 2000). In addition, CO_2 can be used in the presence of a catalyst, such as Ni/Al, to increase the H_2 and CO content (Ollero et al. 2003).

Syngas offers significant flexibility with regard to its utilization. Syngas from coal, known as town gas, was extensively used for lighting and heating during the nineteenth and early part of twentieth centuries. In recent years, there has been renewed interest in the utilization of coal-based syngas for stationary power generation through integrated gasification combined cycle (IGCC) facility (Rodrigues et al. 2003). In addition, it can be used to provide H_2 (Watanabe et al. 2002) or synthesized to produce chemicals and liquid fuels, such as F-T fuels (Tijmensen et al. 2002). The use of syngas in fuel cells, such as solid oxide fuel cells, through the reforming of hydrocarbons and other routes is also being explored (Kee et al. 2005, 2008). Figure 4 in Gill et al. (2011) summarizes the various routes for the utilization of syngas, including the production of F-T and other transportation fuels. Gill et al. (2011) provide an overview of technologies, including Biomass-to-Liquid (BTL) and Coal-to-Liquid (CTL) Gas-to-Liquid (GTL) processes, for producing various fuels through gasification and F-T processes. It should be noted, however, that some of these routes may be more energy intensive, and their cost effectiveness and environmental benefits need to be examined, as it may be more economical to use syngas directly as fuel or for electricity generation.

Biogas or landfill gas (LFG) is typically produced from anaerobic decomposition of organic matter (Gunaseelan 1997). It can also be produced through pyrolysis and gasification processes. Primary sources include biomass, green waste, plant material, manure, sewage, municipal waste, and energy crops. While its composition can vary

significantly depending on the source and production process, the main constituents include CH_4 (50–75 % by volume), CO_2 (25–40 %), N_2 (0–10 %), and small traces of H_2O, O_2, H_2, and hydrogen sulfide, as well as some contaminants such as volatile organic compounds, and halogenated hydrocarbons. Some representative biogas mixtures based on the two common sources, namely agricultural waste and household waste, are provided by Quesito et al. (2013). Like natural gas and syngas, biogas can be used as a transportation fuel in IC engines, or for power generation in gas turbines and boilers. It can also be used as compressed natural gas, or reformed to produce syngas, or in solid oxide fuel cells to generate electricity.

3 Syngas and Biogas Combustion and Emission Characteristics

3.1 Syngas Combustion and Emission Characteristics

Considerable work has been reported on syngas combustion and emission characteristics (Lieuwen et al. 2009; Cheng 2009; Aggarwal 2013). Fundamental studies have focused on various aspects, including the development of thermo-transport and kinetic models, and examining the ignition and combustion characteristics in both laboratory flames and practical devices. A major challenge identified in these studies is due to substantial variation in its composition and heating value. This requires that the fundamental properties, such as adiabatic flame temperature, laminar burning velocity, flammability limits, flame stability, extinction, and blowout, need to be determined for a wide range of syngas composition. This also presents challenges while designing syngas combustors, requiring optimization for locally available fuels. Table 1 lists the heating values and adiabatic flame temperatures (T_{ad}) of various syngas-air mixtures at $\phi = 1.0$. As indicated, T_{ad} is nearly independent of the syngas composition. However, diluents, such as CO_2, H_2O, and N_2, can be used to modify its value. Syngas typically has lower heating values compared to biogas and other hydrocarbon fuels. For example, the higher heating value for syngas with 50 %CO and 50 %H_2 by volume is 18,943 kJ/kg or 284,139 kJ/kmol, while the corresponding values for methane (representative of biogas) are 55,500 kJ/kg and 888,000 kJ/kmol, respectively.

Detailed mechanisms for syngas oxidation have been developed by Davis et al. (2005), Li et al. (2007), Wang et al. (2007), and Kéromnès et al. (2013). Since the oxidation chemistries of H_2 and CO are fundamental to those of hydrocarbon fuels, the mechanisms developed for latter fuels, such as the GRI-3.0 (Smith et al.) and San Diego (2002) mechanisms, have also been used for syngas combustion. Validations for the mechanisms have been provided using ignition delay and laminar flame speed data. Ignition delays have been measured using a variety of devices, including shock tube (Petersen et al. 2007), rapid compression machine (RCM) (Walton et al. 2007), and constant volume (or constant pressure) reactor, while

Table 1 Heating values and adiabatic flame temperatures of syngas mixtures

H_2 mole fraction	CO mole fraction	Mol. weight (kg/kmol)	Heating value kJ/kg	Heating value kJ/kmol	Adiabatic flame temp (ϕ = 1.0) (K)
0	1	28.0	10,101	282,814	2,394
0.2	0.8	22.8	12,428	283,365	2,382
0.4	0.6	17.6	16,130	283,892	2,378
0.5	0.5	15.0	18,943	284,139	2,377
0.6	0.4	12.4	22,933	284,368	2,378
0.8	0.2	7.2	39,539	284,684	2,382
1	0	2.0	141,794	283,588	2,387

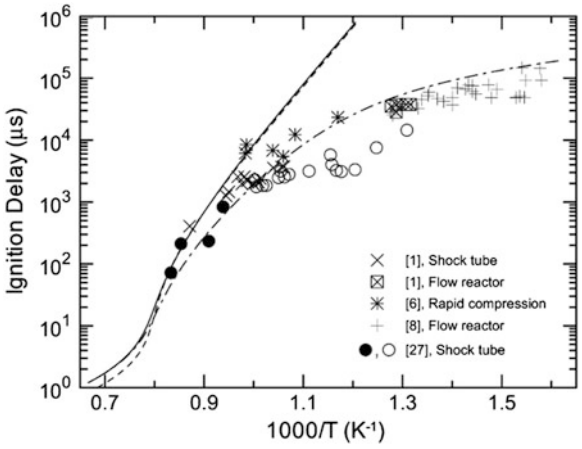

Fig. 2 Ignition delays for various syngas mixtures under different pressure and temperature conditions. *Filled* and *open circles* correspond to strong and weak ignition events, respectively. All experimental data have been normalized to 20 atm assuming $p - 1$ proportionality. *Lines* correspond to ignition delay predictions using the Li et al. mechanism at 20 atm; the *solid line* corresponds to the syngas mixture used in shock tube experiments

computations have often employed a homogeneous reactor configuration (Aggarwal et al. 2011). Figure 2 from Dryer and Chaos (2008) presents some measured and predicted ignition delay data for different syngas mixtures. Additional data can be found in Kéromnès et al. (2013) and other references cited above.

Laminar flame speed represents a fundamental property of a fuel-air mixture. It is of critical importance with regard to burning rate, flame stabilization, flashback, and blowout in practical systems. Laminar burning velocities for H_2–CO mixtures have been measured using different systems, including flat-flame burner (Yan et al. 2001), Bunsen burner (Natarajan et al. 2007, 2009), and expanding spherical flames (McLean et al. 1994; Prathap et al. 2008; Kishore et al. 2011). Figure 3 presents measured and predicted laminar flame speeds versus equivalence ratio and pressure,

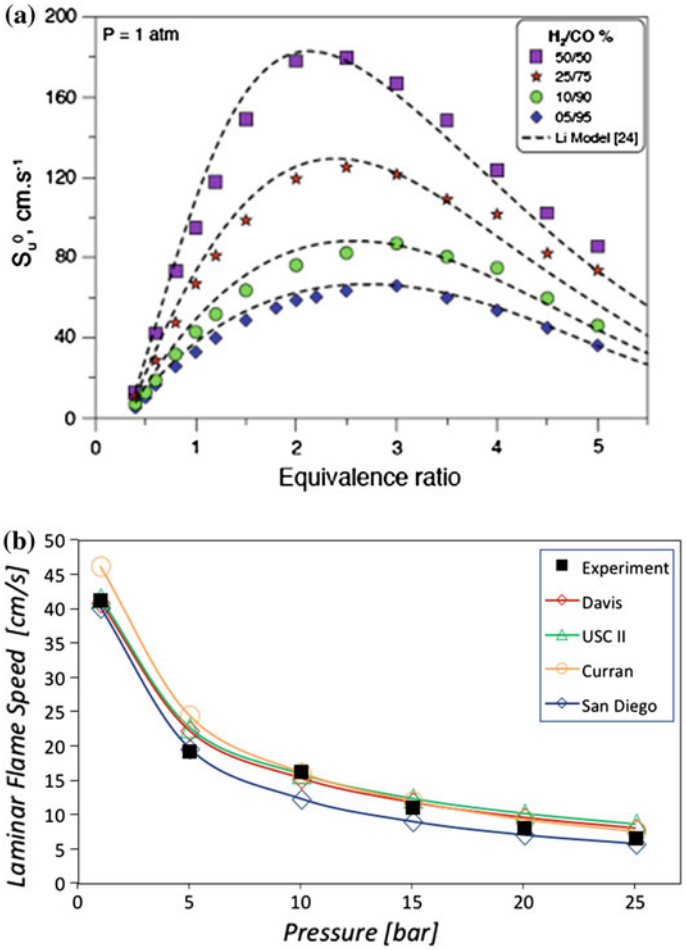

Fig. 3 **a** Measured and predicted laminar flame speeds for various H_2/CO spherically expanding premixed flames. **b** Measured and predicted laminar flame speeds versus pressure at $\phi = 2.5$ for argon-diluted syngas mixture with CO and H_2 mol fractions of 0.265 and 0.029, respectively

respectively. Figure 3a from Bouvet et al. (2011) shows the effect of syngas composition on the burning velocity. As expected, with the increase in H_2 fraction, the flame speed increases, flammability limits become wider, and the peak in flame speed occurs progressively at higher equivalence ratios, ϕ. These effects can be attributed to the higher diffusivity and reactivity of H_2. Figure 3b from Quattrocchi (2014) presents the effect of pressure on the burning velocity. Results are shown for argon-diluted syngas mixture with CO and H_2 mol fractions of 0.265 and 0.029, respectively, at $\phi = 2.5$. Measurements are from Burke et al. (2010), and predictions are performed with the CHEMKIN software using the San Diego (2002), Davis (Davis et al. 2005), USCII (Wang et al. 2007), and Curran (Kéromnès et al. 2013)

mechanisms. McLean et al. (1994) and Vagelopoulos and Egolfopoulos (1998) reported premixed flame speeds at pressures from atmospheric to a few atmospheres. Kéromnès et al. (2013) reported a more extensive study on high-pressure premixed flames. Additional data on syngas flame speeds can be found in the references cited above. In addition to unstretched flame speed, the flame response to stretch and the resulting cellular instabilities are important considerations. These phenomena are of fundamental relevance for flame extinction, turbulent flame propagation, flame stabilization, blowout, and transition to detonation. The flame response to stretch is characterized in terms of the Markstein length or non-dimensional parameter, Markstein number. Spherically expanding flames have been commonly used to determine this parameter, and details can be found in Aggarwal (2013) and Kishore et al. (2011).

Since syngas generally contains other species in addition to CO_2 and H_2O, it is important to examine the effects of various diluents on syngas combustion and emissions. Moreover, dilution is often used to lower the flame temperature and thereby limit NO_x emissions. Several researchers have examined the effects of diluents on laminar flame speed, stability, and emissions (McLean et al. 1994; Natarajan et al. 2009; Kishore et al. 2011; Burke et al. 2007; Burbano et al. 2011; Das et al. 2011). It is important to note that only NO_x emission is relevant in syngas flames, while both soot and NO_x emissions are important for hydrocarbon flames. NO_x in hydrocarbon flames can be formed due to four mechanisms, namely thermal (Zeldovich), prompt (Fenimore), N_2O, and NNH mechanisms (Briones et al. 2007; Guo and Smallwood 2007; Fu et al. 2012). Thermal NO involves reactions: $O + N_2 \Rightarrow N + NO$, and $N + O_2 + NO + O$, and $N + OH \Rightarrow NO + H$, while prompt NO formation is initiated through the reaction $CH + N_2 \Rightarrow NCN$ (or HCN) + H (or N). Thus, the prompt mechanism is absent in syngas flames, since it is linked to hydrocarbon combustion chemistry, which produces CH radicals. The prompt NO, however, may be important for syngas mixtures containing CH_4. The N_2O-intermediate mechanism involves $N_2 + O + M \Rightarrow N_2O + M$ as the initiating reaction and is important for lean mixtures and high pressures. Finally, the NO formation through NNH route involves reactions: $N_2 + H \Rightarrow NNH$ and $NNH + O \Rightarrow NO + NH$ (Bozzeli and Deam 1995). Ding et al. (2011) investigated NO_x formation in lean premixed syngas counterflow flames and observed that the NO was formed predominantly through the NNH and N_2O intermediate routes. The contribution of thermal NO was small due to the low-flame temperatures. In addition, increasing the CO fraction in syngas was found to increase the amount of NO formed.

Combustion in many practical devices involves non-premixed (diffusion) and partially premixed flames (PPFs) (Giles et al. 2006; Som et al. 2008). While numerous studies exist of such flames with hydrocarbon fuels, relatively few investigations have focused on syngas fuel. Studies on non-premixed syngas flames have been reported by Giles et al. (2006), Hui et al. (2007), and Park et al. (2004), while those on PPFs have been reported by Som et al. (2008) and Ouimette and Seers (2009). Giles et al. (2006) also examined the effects of diluents (N_2, H_2O, and CO_2) on NO formation in non-premixed flames. Som et al. (2008) examined the effects of strain rate, equivalence ratio, and syngas composition on the detailed

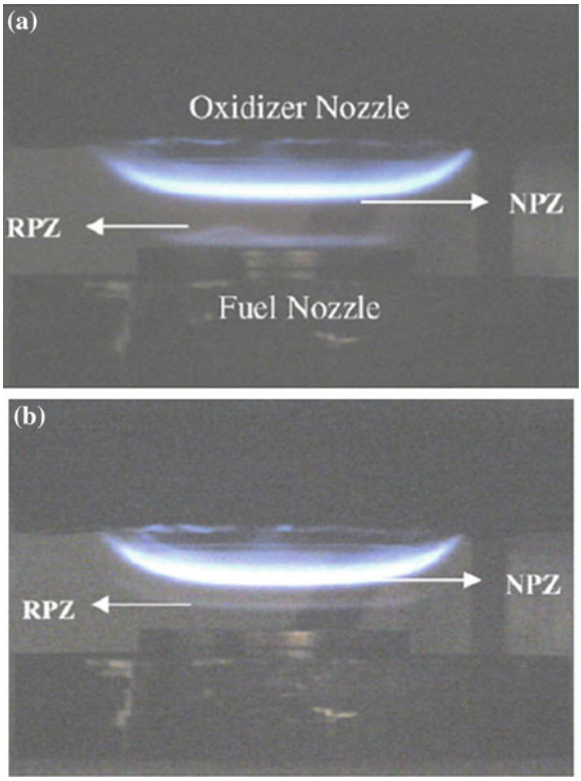

Fig. 4 Images of syngas (50 %H_2/50 %CO)-air partially premixed flames established at ϕ = 6 (**a**) and ϕ = 16 (**b**) in a counterflow burner. Strain rate is 35 s^{-1}

structure and extinction characteristics of PPFs in an opposed-jet burner. Figure 4 from this study depicts images of two such flames established at ϕ = 6 and 16. For ϕ = 6, which is just above the rich flammability limit of 50 %H_2/50 %CO syngas-air mixture, the flame exhibits a typical double flame structure with a weak rich premixed reaction zone (RPZ) established close to the fuel nozzle and a non-premixed reaction zone (NPZ) on the oxidizer side near the stagnation plane. As ϕ is increased, the RPZ moves away from the fuel nozzle, and RPZ and NPZ are much closer to each other. Som et al. also examined the effect of syngas composition and partial premixing on NO emissions.

Ouimette and Seers (2009) reported an experimental investigation on syngas partially premixed jet flames. The effects of ϕ, CO_2 dilution, and H_2/CO ratio on the flame structure and NO_x were reported. Figure 5 from this study presents flame images at different ϕ. As expected, the flame length is strongly influenced by the level of partial premixing. As ϕ decreases from the non-premixed to premixed regime, the flame length decreases monotonically. This has important consequences for the emissions of NO_x, greenhouse gases, and other pollutants, since the flame length directly influences the reacting volume and residence time. In addition, images at 2.0 and 1.6 indicate the existence of two reaction zones, with the NPZ enveloping the RZP. Regarding the NO_x formation, results indicated that $EINO_x$ first increases as ϕ

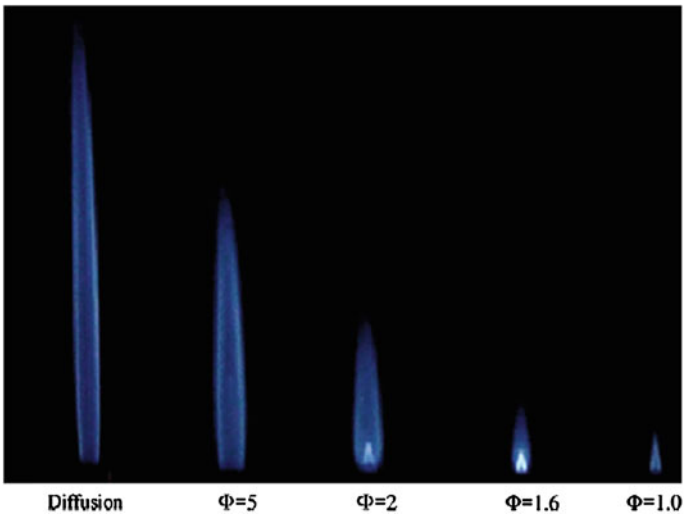

Fig. 5 Images of laminar partially premixed 45 %H_2/35 %CO/20 %CO_2-air flames at different levels of partial premixing. Reynolds number is 1,400

is increased from 1.0 to 1.6, then remains nearly constant for $1.6 < \phi < 3.85$, and subsequently decreases slowly as ϕ is increased to the diffusion limit ($\phi \Rightarrow \infty$).

Studies on turbulent syngas flames have focused on the determination of turbulent flame speeds (S_T); (Daniele et al. 2011; Venkateswaran et al. 2011; Monteiro et al. 2011). Venkateswaran et al. (2011) reported measurements of global turbulent flame speeds using a Bunsen burner and examined the effects of ϕ, syngas composition, mean flow velocity, and turbulence intensity. Consistent with other studies, the flame speed was found to exhibit sensitivity to fuel composition over a wide range of turbulence intensity, increasing significantly with the increase in H_2 content. The data were further analyzed to develop flame speed correlations, indicating the effects of thermo-diffusive instabilities through negative Markstein lengths.

3.2 Biogas Combustion and Emission Characteristics

There have been few studies focusing directly on biogas combustion. However, there is a large body of literature on methane combustion, including ignition, extinction, flammability limits, flame speeds, cellular instabilities, and emissions. Consequently, detailed thermo-transport and kinetic models have been developed to simulate and analyze methane flames in a variety of configurations. Considerable research has also been reported on the extinction and blowout of methane-air flames using various diluents, such as CO_2, N_2, H_2O, and chemical agents (Linteris et al. 2008; Aggarwal 2009). Most of these studies and the associated models can be readily used for analyzing the combustion and emission characteristics of biogas, whose main

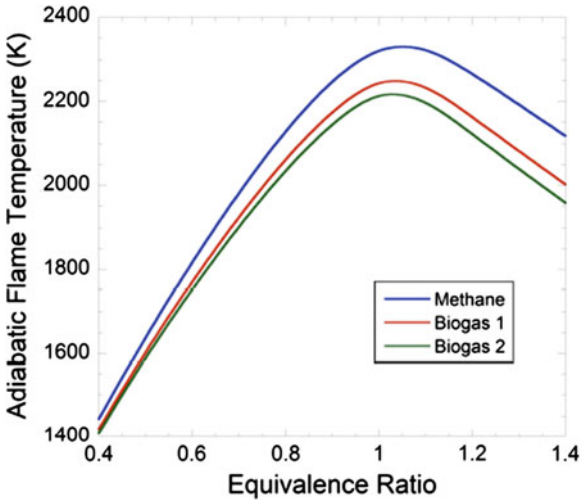

Fig. 6 Computed adiabatic flame temperatures of methane-air and two biogas-air mixtures. Pressure = 1 atm and initial temperature = 500 K

constituents are CH_4 and CO_2 with small traces of H_2O and N_2. This section provides a brief overview of the fundamental combustion and emission properties of biogas.

Biogas has lower energy content compared to natural gas. For example, the volumetric heating values of natural gas (94 %CH_4) and biogas (60 %CH_4/40 %CO_2) are 38.6 and 25 MJ/m^3, respectively. This has consequences for using biogas in natural gas-fired combustion devices, since lower heating value implies higher feeding rates and lower flame temperatures. Figure 6 compares the computed adiabatic flame temperatures for methane-air and two representative biogas-air mixtures. The compositions of these two mixtures, which represent the common feedstock, are 68 %CH_4/26 %CO_2/5 %H_2O/1 %N_2 and 60 %CH_4/33 %CO_2/6 %H_2O/1 %N_2, respectively. As indicated, the biogas flame temperature is about 100–200 K lower than that of methane, depending upon the feedstock biogas. Lower temperatures imply lower flame speeds and thermal NO for biogas flames compared to those for methane flames. The comparison of laminar burning speeds for freely propagating methane and biogas flames is shown in Fig. 7, which shows the flame speed as a function of equivalence ratio and pressure. The flames were computed using the CHEMKIN software and the GRI-3.0 kinetic mechanism. As expected, flame speeds are lower for biogas-air mixtures compared to those for methane-air mixtures. The effect of pressure on flame speed is qualitatively similar for all the three cases shown, with the flame speed first decreasing sharply and then increasing relatively slowly with increase in pressure.

Since biogas is potentially a cleaner and sustainable alternative to natural gas, it is relevant to analyze the emission characteristics of methane and biogas flames in different combustion regimes. Figure 8 from Quesito et al. (2013) compares the computed NO, NO_2, and C_2H_2 profiles in methane and biogas-air PPFs. These flames were simulated in a counterflow geometry at fuel stream equivalence ratio

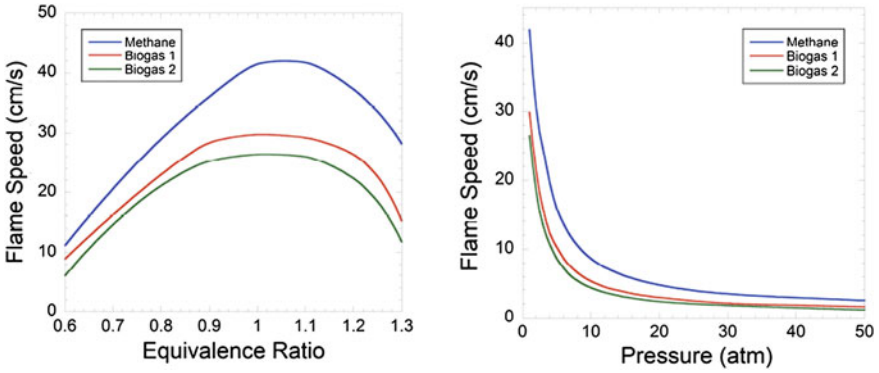

Fig. 7 Computed laminar flame speeds of methane-air and two biogas-air mixtures. Flame speed is plotted versus ϕ (*left*) and pressure (*right*)

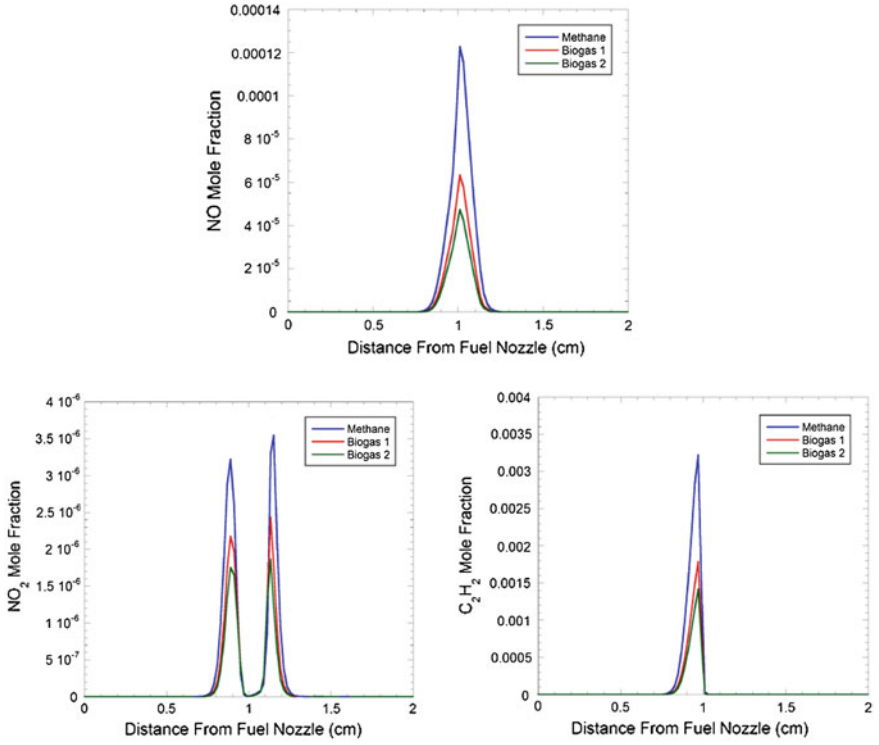

Fig. 8 NO, NO_2, and C_2H_2 mole fraction profiles in counterflow partially premixed flames burning methane and two biogases

ϕ = 3, pressure = 1 atm, and strain rate = 200 s^{-1}, using the Chemkin software and GRI-3.0 mechanism. For all three cases, the flames exhibited a double flame structure with a RPZ located on the fuel side (at about 0.9 cm from the fuel nozzle) and a NPZ on the oxidizer side near the stagnation plane (at about 1.05 cm from the fuel nozzle). These two reaction zones are clearly seen in the NO_2 profiles. The NO and NO_2 profiles indicate significantly lower level of NO_x formation in biogas flames compared to that in methane flames. This may be attributed to the less thermal NO and prompt NO formed, indicated by lower temperatures and C_2H_2 peaks, in biogas flames compared to those in methane flames. The lower C_2H_2 peaks also imply lower prompt NO and soot formation in biogas flames, although soot emission is not a major concern in natural gas and biogas flames.

3.3 Syngas and Biogas Combustion in Practical Devices

There have been numerous studies in recent years dealing with various aspects of syngas-fueled combustion systems. Many of these studies are discussed in a special issue of Combustion Science and Technology (2008). There is significant interest in using syngas in gas turbine engines (Luessen 1997; Lieuwen et al. 2008; Dam et al. 2011), especially in the context of an IGCC facility, for efficient, low-emission power generation, and for carbon capture and storage. Extensive literature exists dealing with the natural gas (NG)-fired combustors, which is beyond the scope of this review. Some research in this area has also focused on using syngas in natural gas-fired combustors (Colantoni et al. 2010). The viability of using syngas and biogas in spark ignition (SI) and compression ignition (CI) engines has been a subject of numerous investigations (Boehman and Le Corre 2008; Sahoo et al. 2012; Bika et al. 2011; Korakianitis et al. 2011). With regard to CI engines, much of the research has focused on dual-fuel operation, which is discussed in the next section. The use of syngas in SI engines offers many advantages, such as better anti-knocking properties and operation with leaner mixtures. Improved knock resistance is due to the presence of CO and enables operation at higher compression ratio, leading to higher thermal efficiency. However, higher burning rate due to the presence of H_2 can lead to higher end gas temperature and increased propensity to knocking. The presence of H_2 can also increase NO_x emissions, which may be controlled by using leaner mixtures (Boehman and Le Corre 2008). Bika et al. (2011) examined such issues by performing single-cylinder experiments for different syngas compositions, compression ratios, and equivalence ratios. For a given ϕ and spark timing, the knock-limited compression ratio was observed to increase with increasing CO fraction. The burn duration and ignition lag also increased with increasing CO fraction.

Compared to CI engines, the NG-fueled SI engines for automobiles have been used with reasonable success, especially in South America. For instance, there are nearly 3.4 million natural gas vehicles (NGVs) in operation in Brazil and Argentina. A number of studies have examined the performance and emission characteristics of

biogas- and NG-fueled SI engines (Korakianitis et al. 2011; González et al. 2013). The advantages of NG or biogas are due to their higher octane number, lower cost, and reduced GHG and particulate emissions. Thus compared with conventional gasoline engines, SI engines using natural gas can run at higher compression ratios, thus producing higher thermal efficiencies and lower CO_2 emissions. However, NO_x, CO, and UHC emissions may be higher, and such engines produce less power than gasoline-fueled engines due to a combination of factors, including lower volumetric efficiency due to natural-gas injection in the intake manifold, lower stoichiometric fuel/air ratio of natural gas compared to gasoline, and the lower equivalence ratio at which these engines may be run in order to reduce NO_x emissions. In addition, high-pressure storage tanks are required to replace the liquid-fuel tank of a conventional vehicle, and fuel injectors or fuel induction systems need to be modified due to higher flow rates required to overcome the low density of natural gas. Despite these modifications, NGVs cannot operate over the same distances as conventional vehicles due to the much lower energy content of NG per unit volume.

In summary, more experimental and computational studies are needed to optimize the engine performance and emissions for various operating conditions and syngas and biogas composition. Research should also focus on examining the use of syngas and biogas in new engine designs, such as Homogeneous Charge Compression Ignition (HCCI) and low temperature combustion.

4 Use of Syngas and Biogas in Dual-Fuel Diesel Engines

Numerous studies have examined the viability of a dual-fuel or blended-fuel strategy using a variety of liquid and gaseous fuels for transportation and power generation. Such blends include bio/petroleum (Hansen et al. 2005), H_2-gasoline (Changwei and Shuofeng 2009), H_2-NG (Ma et al. 2007; Wang et al. 2008a; Das et al. 2000; Kahraman et al. 2009; Dimopoulos et al. 2008; Morrone and Andrea 2009), H_2-CH_4 (Bauer and Forest 2001a, b), H_2-diesel (Shirk et al. 2008), and syngas-diesel (Boehman and Le Corre 2008; Sahoo et al. 2012). The use of NG or biogas in dual-fuel mode has also been investigated using spark SI (Cho and He 2007; Chandra et al. 2011), CI (Duc and Wattanavichien 2007; Ryu 2013), and HCCI (Naber et al. 1994) engines. In diesel engines, a gaseous fuel-air mixture is introduced through the intake valve, while the diesel fuel is injected and compression ignited. Research has focused on the effect of a gaseous fuel on the performance and emission characteristics of gasoline or diesel engines. The effects of various parameters, such as fuel composition, blending ratio, injection timing, EGR, and gaseous fuel-air ratio, have been characterized at different loads. While a number of aspects have been examined (Liu et al. 2003, 2013; Shah et al. 2011; Sahoo et al. 2009), a common observation is that a dual-fuel strategy with NG-diesel at high loads leads to lower PM, CO_2, and volatile organic compounds (VOC) emissions, but somewhat higher CO and UHC emissions, and that the engine power may be reduced due to lower volumetric energy content of NG, although similar thermal efficiency can be maintained. The benefits of dual-fuel

operation become less clear at low loads, and issues concerning reduced engine power and higher UHC and CO emissions need to be addressed by optimizing other parameters, i.e., injection timing, EGR, amount of liquid (pilot) fuel injected, and gaseous fuel equivalence ratio (Chatlatanagulchai et al. 2010a, b; Tomita et al. 2009). Engine experiments using syngas-diesel combination (Boehman and Le Corre 2008; Sahoo et al. 2012) indicated that the engine performance and emissions are strongly influenced by the syngas composition, depending upon the load and other conditions. In general, increasing H_2 fraction in syngas was found to improve engine performance, reduce CO and hydrocarbon emissions, but increase NO_x emissions.

The literature review indicates extensive experimental research dealing with dual-fuel (NG-diesel and syngas-diesel) CI engines, but relatively few computational studies on this topic (Singh et al. 2006; Shah et al. 2011). In particular, many details of the two-stage ignition process, different combustion modes, and emission characteristics in dual-fuel engines remain unexplored. Motivated by this consideration, we performed a numerical investigation on the effect of gaseous fuels on the ignition, combustion, and emissions in a dual-fuel diesel engine. The following sections provide a brief description of the computational model, and some representative results focusing on the two-stage ignition behavior, various combustion models including lean premixed burning and extinction, and emissions.

4.1 Computational Model

Simulations were performed using a 3D CFD software CONVERGE (Senecal et al. 2003), which incorporates state-of-the-art models for spray injection, breakup and atomization, turbulence, droplet collision and coalescence, spray-wall interaction, and vaporization. Details of these models are provided elsewhere (Senecal et al. 2007). The mathematical model is based on Eulerian-Lagrangian formulation for the two-phase turbulent reacting flow. The gas-phase flow field is described using the Favre-averaged Navier-Stokes equations along with the RNG k-ε turbulence model. The spray is represented by a stochastic system of a discrete number of parcels, which are tracked computationally using a Lagrangian scheme. The two phases are coupled through the mass, momentum, and energy exchange terms, which are present in both the liquid- and gas-phase equations. The injection process is simulated using a blob injection model, which injects liquid droplet parcels with a diameter equal to an effective nozzle diameter. The subsequent breakup process is simulated by using models based on the Kelvin-Helmholtz (KH) and Rayleigh-Taylor (RT) instabilities (Patterson and Reitz 1998). The droplet evaporation model is based on the Nusselt number and Sherwood number correlations of Chiang et al. (1992). The CFD solver uses an innovative modified cut-cell Cartesian method along with an adaptive mesh resolution technique for grid generation (Richards et al. 2013).

Computations consider a 1.9L 4-cylinder GM light-duty diesel engine, which has been extensively used for experimental studies at Argonne National Laboratory (Ciatti and Subramanian 2011). The engine has a 7-hole common-rail injector in

Table 2 Engine parameters and other properties for the reference case

Engine speed, rpm	1,500
Engine bore diameter, mm	82
Engine stroke length, mm	90.4
Squish height, mm	0.6
Connecting rod length	145.4
IVC (intake valve closing), CAD	−132 ATDC
Gas temperature at IVC, K	350
Gas pressure at IVC, bar	1.23
EVO (exhaust valve opening), CAD	116 ATDC
SOI (start of injection), CAD	−8 ATDC
Fuel injection temperature, K	298
Nozzle diameter, mm	0.141
Injection duration, CAD	8.5
Fuel intake temperature, K	298
Cylinder head temperature, K	500
Cylinder wall temperature, K	450
Piston wall temperature, K	550

each cylinder. Simulations were performed for a 1/7 (51.43°) sector of the cylinder. Table 2 provides the engine parameters and other properties for the reference case. N-heptane is used as the surrogate for diesel fuel, while methane is used to represent biogas. For dual-fuel cases, methane or syngas premixed with air is introduced through the intake manifold. Simulations are started at the intake valve closing. The fuel oxidation chemistry is modeled using the Chalmers mechanism (Golovichev n. d.; Tao et al. 2007), which contains 42 species and 168 reactions. The software also contains models for soot and NO_x formation, which are described by Senecal et al. (2007) and Patterson and Reitz (1998).

While the reaction mechanism has been extensively validated in previous studies, additional validation is provided in Fig. 9, which presents the predicted and measured ignition delays for n-heptane/air, methane/air, and syngas/air mixtures at engine relevant conditions and $\phi = 1$. The constant pressure homogeneous reactor simulations were performed using the CHEMKIN software along with the Chalmers and CRECK (Ranzi 2012) mechanisms. The CRECK mechanism is a comprehensive mechanism with 466 species 14,631 reactions and has previously been validated against various targets, including ignition delays, flame speeds, and species measurements. In the figure, the predicted ignition delays are compared against the measurements for n-heptane/air (Gauthier et al. 2004), methane/air (Huang et al. 2006), and syngas/air mixtures (Mittal et al. 2006). Overall, there is good agreement between the measurements and predictions of the two mechanisms. The Chalmers mechanism somewhat overpredicts ignition delays for n-heptane and underpredicts for methane at high temperatures. For syngas, both the mechanisms significantly underpredict the ignition delay at temperatures below 1,000 K. These differences have been attributed to mixture non-homogeneities present in

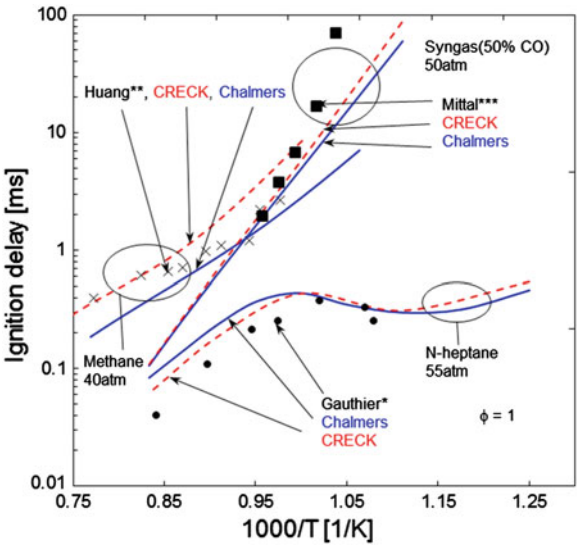

Fig. 9 Predicted and measured ignition delays for n-heptane/air, syngas/air, and methane-air mixtures at high pressures and $\phi = 1$

experiments, but were not duplicated in simulations (Dryer and Chaos 2008; Jain et al. 2013). It is also noteworthy that the Chambers mechanism is able to reproduce the experimentally observed two-stage ignition process and negative temperature coefficient (NTC) region.

4.2 Ignition Characteristics in Dual-Fuel Diesel Engines

In a dual-fuel engine, the ignition is initiated by the pilot diesel. Since ignition represents a critical process with regard to engine performance and emissions, it is important to examine the ignition of pilot fuel in the presence of a combustible gaseous fuel-air mixture. In particular, the ignition chemistry of large hydrocarbons, such as n-heptane, is known to be characterized by the NTC (negative temperature coefficient) and two-stage ignition processes (Curran et al. 1998). Previous studies have not analyzed the effect of gaseous fuels on these processes. Therefore, simulations were performed to examine these aspects by considering homogeneous gaseous mixtures in a constant volume reactor and two-phase mixtures in a diesel engine. Figure 10 depicts the first and second stage ignition processes in diesel engine in terms of the mass profiles of OH and QOOH with respect to crank angle for the single- and dual-fuel cases, as listed in Table 3. As indicated in the table, the start of injection (SOI) is −8° after top dead center (ATDC), and injection duration is 8.5 crank angle degree (CAD).

For n-heptane, the two-stage ignition process is well depicted in the figure, with the first-stage ignition occurring at −4.8° ATDC and the second-stage at −2.4° ATDC. The first-stage ignition is defined by the value of integrated heat release

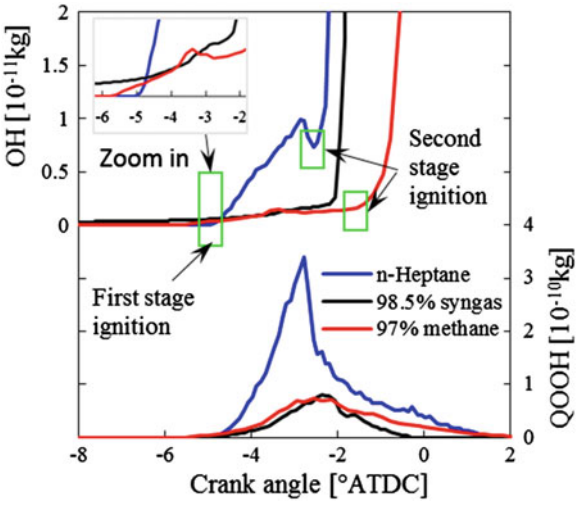

Fig. 10 Integrated mass profiles of OH and $C_7H_{14}OOH$ (QOOH) for single-fuel (n-heptane), 97 % methane, and 98.5 % syngas dual-fuel cases in diesel engine. The *green rectangles* indicate the first- and second-stage ignitions

Table 3 Input parameters, and computed performance and emission parameters for single- and dual-fueled engine simulations

	Low load			High load	
Mole fraction of methane	0 %	90 %	0 %	97 %	0 %
Mole fraction of syngas (50 % CO, 50 % H_2)	0 %	0 %	95 %	0 %	98.5 %
Mole fraction of n-heptane	100 %	10 %	5 %	3 %	1.5 %
Total chemical energy per cylinder, J	390			1,014	
Mass of n-heptane per cylinder, mg	8.8	3.3	3.3	3.3	3.3
Mass of methane per cylinder, mg	0	4.8	0	17.3	0
Mass of syngas per cylinder, mg	0	0	13.8	0	50
Mass of air per cylinder, mg	546	542	532	515	456
ϕ based on gaseous fuel	0	0.16	0.17	0.58	0.60
Total volume per cylinder, L	0.448				
Work output per cylinder, J	133	87	95	351	228
Indicated mean effective pressure (*IMEP*), bar	2.78	1.82	1.98	7.36	4.77
CA50 (°ATDC)	1.3	3.6	3.2	5.4	-0.4
Indicated power, kW	1.66	1.09	1.18	4.39	2.85
Engine efficiency (%)	34	22	24	35	22
Specific soot emission (mg/kWh)	15.3	2.2	1.8	1.8	0.6
Specific NO_x emission (g/kWh)	0.51	0.52	0.66	0.89	3.58
Specific UHC emission (g/kWh)	0.21	9.46	0.12	1.81	0.00
Specific CO emission (g/kWh)	0.30	1.76	19.88	0.14	0.00

The emission values are at exhaust valve open (EVO) crank angle

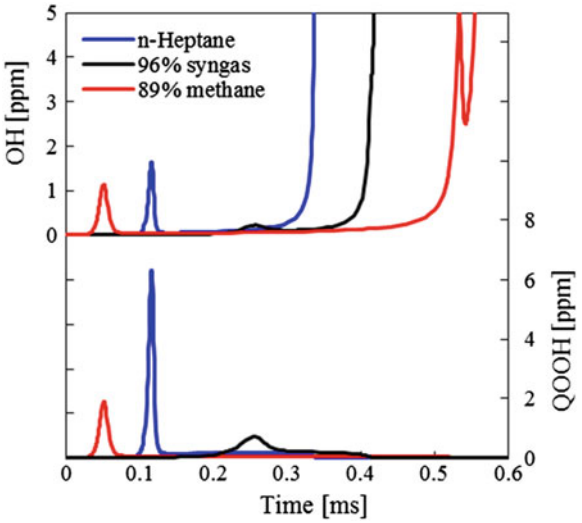

Fig. 11 Temporal profiles of OH, $C_7H_{14}OOH$ (QOOH), and HO_2 mol fraction for single-fuel (n-heptane), 89 % methane and 96 % syngas dual-fuel cases in homogeneous constant volume reactor (CHEMKIN). Simulations for the dual-fuel cases are carried out using the same gaseous equivalence ratios as those for engine simulations discussed in the context of Fig. 10. The n-heptane mole fraction in the initial mixture is specified using a global $\phi = 1$

(IHR) exceeding 0.01 J, while the inflection point in the heat release rate (HRR) profile (not shown) defines the second-stage ignition. These ignition delay values are consistent with those determined from the QOOH and OH profiles shown in Fig. 10, where the first rise in either OH or QOOH indicates the first-stage ignition and the second (sharp) rise (after the first peak) in OH indicates the second stage. The use of QOOH and OH profiles to identify the first and second stage ignition was further confirmed by performing CHEMKIN simulations in homogeneous constant volume reactor. As indicated by the species temporal profiles for n-heptane in Fig. 11, the first sharp rise or peaks in QOOH and OH profiles marks the first stage of ignition, while the second sharp rise in OH marks the second stage ignition. The first and second ignition delays were also confirmed using the 3D contour plots of QOOH and OH mass fractions (not shown). For the dual-fuel case with methane, the first- and second-stage ignition crank angles from Fig. 10 are −5.2° ATDC and −1.2° ATDC. Note, however, that the first ignition is not clearly distinguishable for the engine case (Fig. 10), but can be seen for the homogeneous mixture (Fig. 11). In contrast, the first-stage ignition for the syngas dual-fuel case is not clearly visible for either engine or homogeneous mixture simulations. Another important observation from Figs. 10 and 11 is that for the homogeneous mixture, the presence of gaseous fuel (methane or syngas) increases the ignition delay for the dual-fuel cases compared to single fuel. However, the ignition delay is not affected noticeably by the presence of gaseous fuel in engines, and this can be attributed to the spatially and temporally evolving species and temperature fields in engines sprays.

4.3 Combustion and Emission Characteristics of Dual-Fuel Diesel Engines

Simulations were performed for one single-fuel case (100 % n-heptane), and four dual-fuel cases, two with methane (90, and 97 % by volume), and the other two with 95 and 98.5 % syngas (50 %CO-50 %H_2). As indicated in Table 3, cases with 100 % n-heptane, 90 % methane, and 95 % syngas correspond to low-load condition for which the total (fuel) energy into the cylinder is 390 J. The other two cases with 97 % methane and 98.5 % syngas correspond to high-load condition with total energy into the cylinder being 1,014 J. Also, for the two low-load cases, the gaseous equivalence ratios are ϕ_g = 0.16 and 0.17, while for the two high-load cases, ϕ_g = 0.58 and 0.60.

Figure 12 depicts the combustion characteristics for the 0, 90, and 97 % methane cases in terms of the temporal profiles of pressure, HRR, n-heptane vapor mass, and methane mass. For the first two cases corresponding to low-load condition, the amount of energy input is kept fixed, whereas for the 90, and 97 % methane cases, the amount of n-heptane injected is kept fixed. Thus, with the increase in methane mass, the indicated mean effective pressure (IMEP) increases from 1.88 to 7.36 bar, as indicated in Table 3. The increased load for the 97 % methane can also be seen from the pressure and HRR plots in Fig. 12. In addition, the HRR plots indicate that the ignition delay is increased due to the addition of methane, as discussed earlier.

The combustion process in a diesel engine is generally characterized by a hybrid combustion mode involving rich premixed combustion and diffusion combustion (Dec 1997; Som and Aggarwal 2010). In contrast, depending upon operating conditions, the heat release in a dual-fuel engine may also involve a lean combustion mode with a propagating flame (Boehman and Le Corre 2008). The HRR and methane mass profiles in Fig. 12 seem to support this hypothesis, especially for the 97 % methane case. However, the methane mass profile for the 90 % case seems to indicate the extinction of the lean premixed flame due to ultra lean conditions at low load. Various combustion modes and the flame propagation/extinction behavior were analyzed by examining the evolution of some key species during combustion. Figure 13 presents the CO, CO_2, and HO_2 mass fraction contours at different crank angles for the single-fuel case. These plots are cut through at the peak ϕ value location. Black lines in each figure indicate ϕ contours (0.3–3). The corresponding plots for the two duel-fuel cases are shown in Figs. 14 and 15. These plots can be used to identify the different combustion zones. For instance, the high CO region locates the rich premixed zone with ϕ between 2.0 and 3.0, while the high CO_2 region corresponds to diffusion combustion zone with ϕ near 1. This is consistent with previous studies (Azzoni et al. 1999; Aggarwal 2009) dealing with PPFs, indicating that the most of CO is produced in the rich premixed zone, while the most of CO_2 is produced in the diffusion combustion zone, where the temperature is highest. Thus, the rich premixed zone is characterized by n-heptane decomposition and partial oxidation, producing CO, H_2, and intermediate hydrocarbon species. These species are then consumed through oxidation reactions in the diffusion

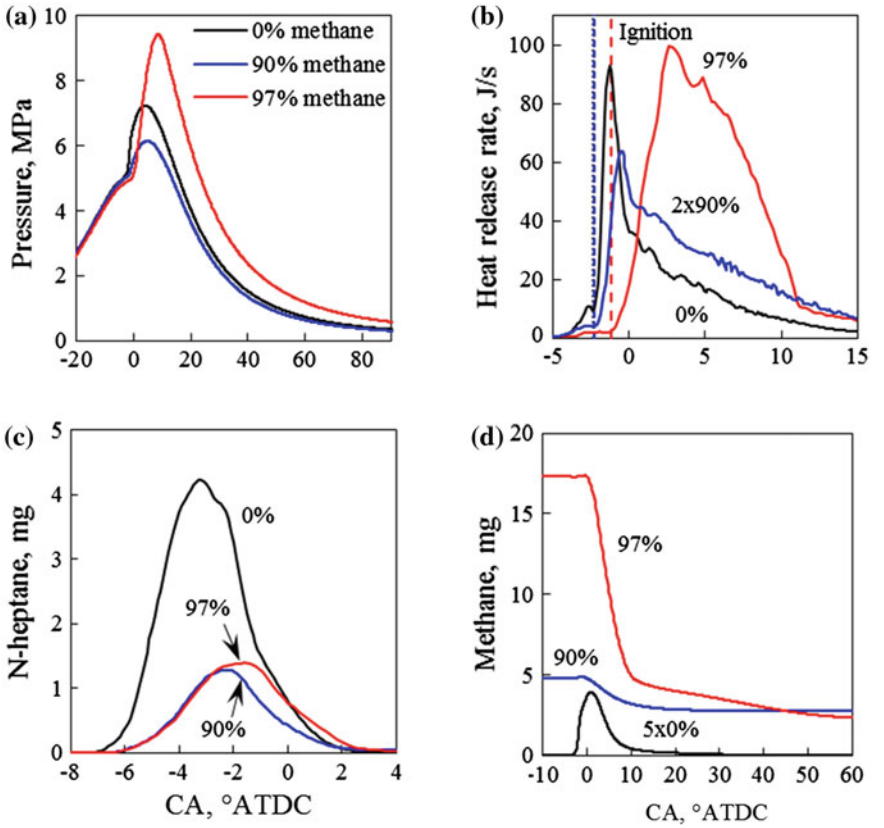

Fig. 12 Pressure, heat release rate, n-heptane vapor, and methane mass profiles with respect to crank angle for the 0 % (100 % n-heptane), 90 and 97 % methane cases. *Vertical lines* in **b** indicate crank angles at ignition

combustion zones. In a similar way, HO_2 plots can be used to examine the lean combustion zone. Thus, for the two dual-fuel cases, HO_2 contours at 0 and 4° ATDC (cf. Figs. 14 and 15) indicate the presence of a lean combustion zone, characterized by a propagating flame. However, the corresponding contours for the single-fuel case do not show this lean combustion zone (cf. Fig. 13).

The three combustion zones for the dual-fuel combustion can be qualitatively identified by deconstructing the HRR diagram based on the temporal mass profiles of some relevant species. Figure 16 presents the mass profiles of several such species for the 97 % methane case. As indicated, the rich premixed combustion mostly occurs between −5° and 3° ATDC and is characterized by the consumption of n-heptane and the production of C_2H_2, CO, and other intermediate species, such as H_2. As indicated in Fig. 16a, C_2H_2 and CO species attain their peak values during this period. Based on this observation, a HRR profile corresponding to rich premixed combustion can be constructed and is shown in Fig. 16b. Similarly, from the

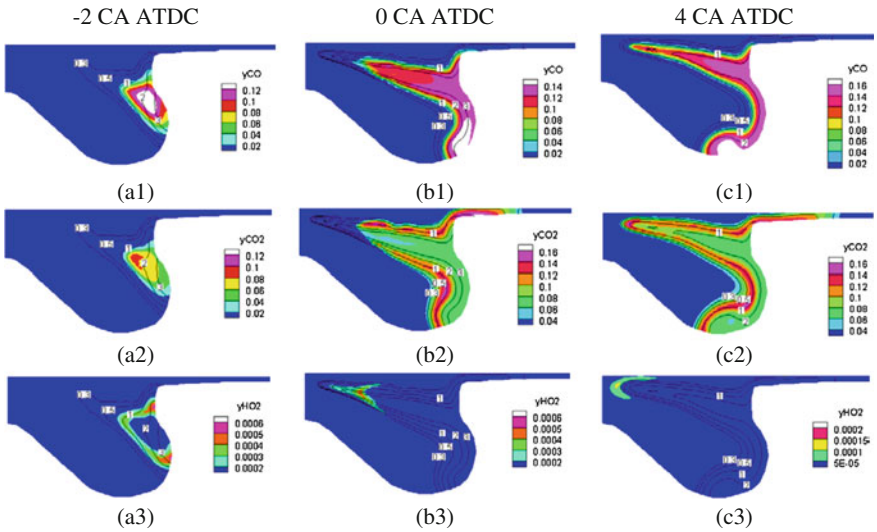

Fig. 13 CO (*a1–c1*), CO_2 (*a2–c2*), and HO_2 (*a3–c3*) mass fraction contours for the n-heptane case at −2, 0, and 40 ATDC. Black lines in each figure indicate ϕ contours (ϕ = 0.3–3)

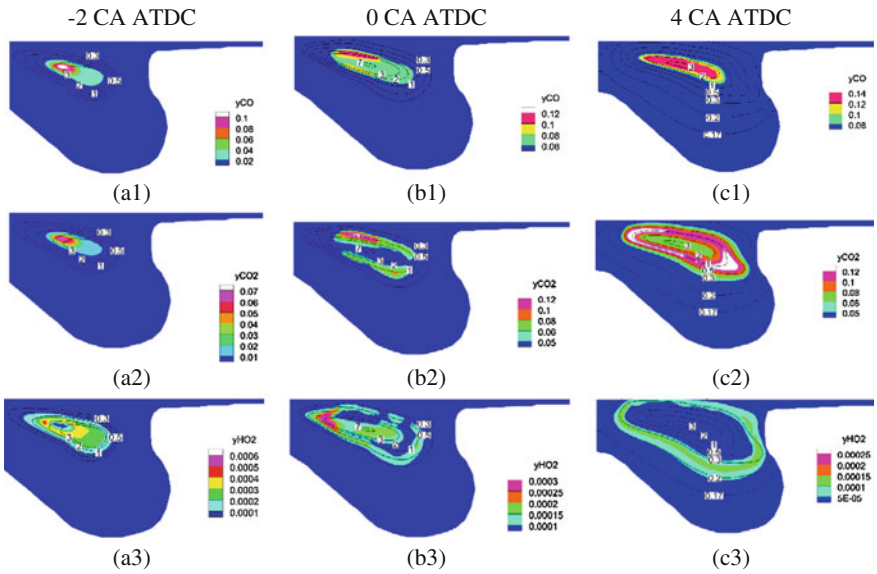

Fig. 14 CO (*a1–c1*), CO_2 (*a2–c2*), and HO_2 (*a3–c3*) mass fraction contours for the 90 % methane dual-fuel case at −2, 0, and 40 ATDC. Black lines in each figure indicate ϕ contours (ϕ = 0.3–3)

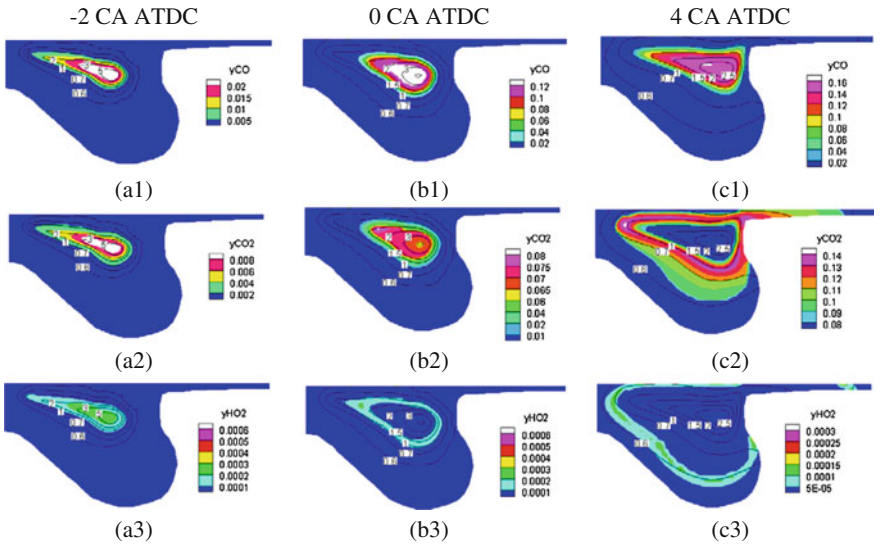

Fig. 15 CO (*a1–c1*), CO_2 (*a2–c2*), and HO_2 (*a3–c3*) mass fraction contours for the 97 % methane dual-fuel case at −2, 0, and 40 ATDC. *Black lines* in each figure indicate ϕ contours (ϕ = 0.3–3)

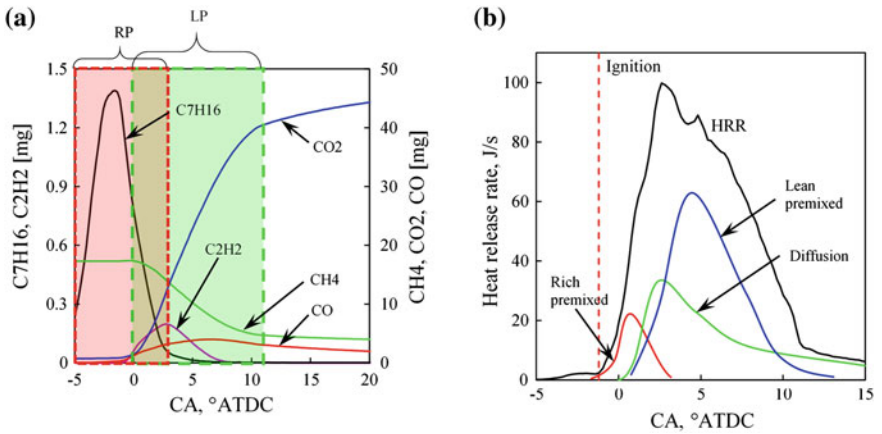

Fig. 16 **a** Temporal mass profiles of n-C_7H_{16}, C_2H_2, CH_4, CO, and CO_2 for the 97 % methane case and **b** Computed HRR for the engine combustion and qualitative HRR profiles for the rich premixed, diffusion, and lean premixed combustion, constructed based on the species profiles

methane mass profile, the duration for the lean premixed combustion can be defined to be between 0° and 10° ATDC. Methane is almost completely consumed during this period, producing a significant amount of CO_2. Accordingly, a HRR profile for lean combustion can be constructed and is also shown in Fig. 16b. Finally, C_2H_2, CO, and other species (such as H_2), which are produced during rich premixed combustion, are consumed in the diffusion combustion zones. Consequently, the

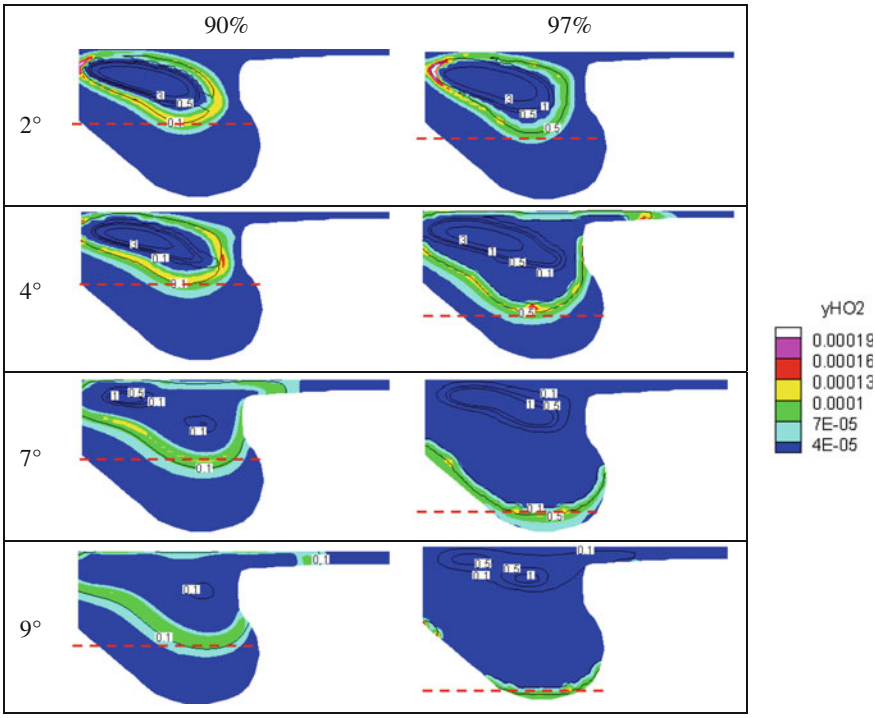

Fig. 17 HO_2 mass fraction contours at different crank angles for the 90 and 97 % methane cases. *Black lines* indicate ϕ contours. *Red line* in these figures shows the flame propagation

HRR profile corresponding to diffusion combustion can be constructed based on this observation and the overall HRR profile. This is also shown in Fig. 16b. The diffusion combustion is estimated to occur between 0° and 60° ATDC, during which time CO_2 (cf. Fig. 16a) and H_2O attain their peak values.

As stated earlier, the methane profiles (Fig. 12) indicate the extinction of lean combustion zone for the 90 % methane case. This is further confirmed by analyzing the HO_2 contours presented in Fig. 17 for the two dual-fuel cases. For both cases, the contours at 2° ATDC indicate the presence of a lean propagating flame in the piston bowl. For the 90 % methane case, however, the HO_2 contours at 7° and 9° ATDC indicate that the flame is extinguished due to ultra lean conditions, with $\phi \approx 0.05$–0.1 ahead of the flame, and due to the fact that pressure and temperature decrease during the expansion stroke. In contrast, the contours for the 97 % case indicate a lean propagating flame with $\phi \approx 0.5$. Consequently, most of methane gets consumed through lean premixed combustion for this case, while a significant amount of methane remains unreacted for the 90 % case. This is further confirmed by the methane profiles discussed earlier in the context of Fig. 12. Note that a small amount of methane remains unreacted for the 97 % case, but it is mostly confined to the crevice and boundary layer regions. These regions also contribute to UHC and CO emissions.

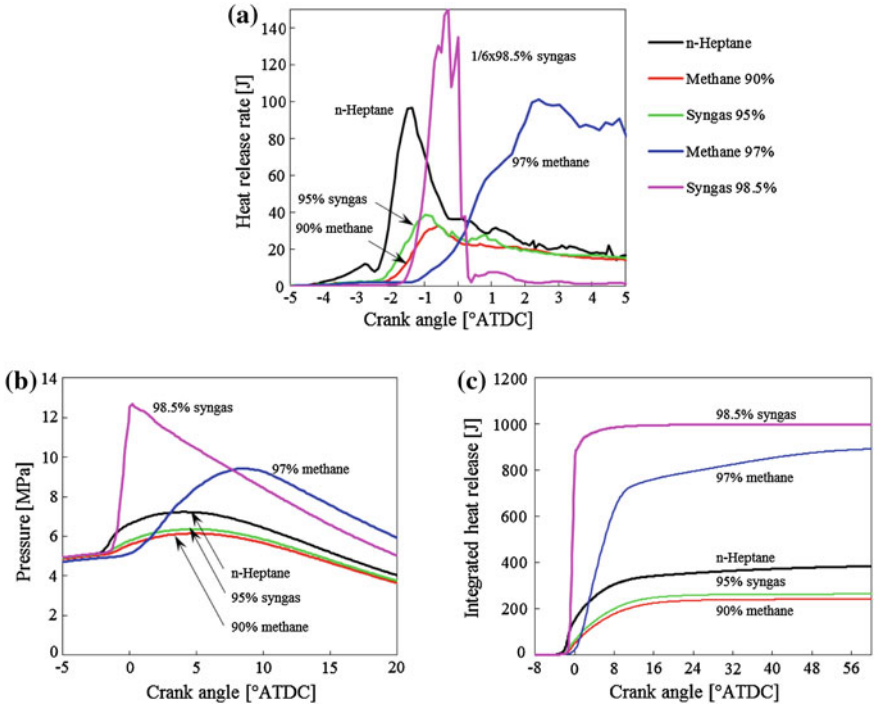

Fig. 18 Heat release rate (**a**), pressure (**b**), and IHR (**c**) profiles with respect to crank angle for the single fuel (n-heptane), and 90 and 97 % methane dual-fuel, and 95 and 98.5 % syngas dual-fuel cases

Results for the syngas dual-fuel cases are shown in Fig. 18, which plots the HRR, pressure, and IHR profiles for all the five cases. The HRR and pressure profiles for the low-load cases (90 % methane and 95 % syngas) indicate more rapid combustion and higher heat release for 95 % syngas compared to that for 90 % methane. Consequently, as indicated in Table 3, IMEP and engine efficiency are higher for 95 % syngas compared to those for 90 % methane. Differences between the syngas and methane become significantly more pronounced at high-load condition (97 % methane and 98.5 % syngas). The HRR and pressure profiles for syngas indicate nearly spontaneous combustion with a very sharp rise in heat release and pressure but a gradual combustion process for methane. The total heat release is also noticeably higher for syngas compared to that for methane. These differences are primarily due to the much faster flame propagation in syngas-air mixture compared to that in methane-air mixture, even though the equivalence ratios for the two mixtures are nearly the same (Table 3).

The flame propagation behavior is illustrated in Fig. 19, which presents the HO_2 contours for the 95 and 98.5 % syngas cases. Similar to the methane case, the contour plots are cut through the peak ϕ value location. As expected, the plots

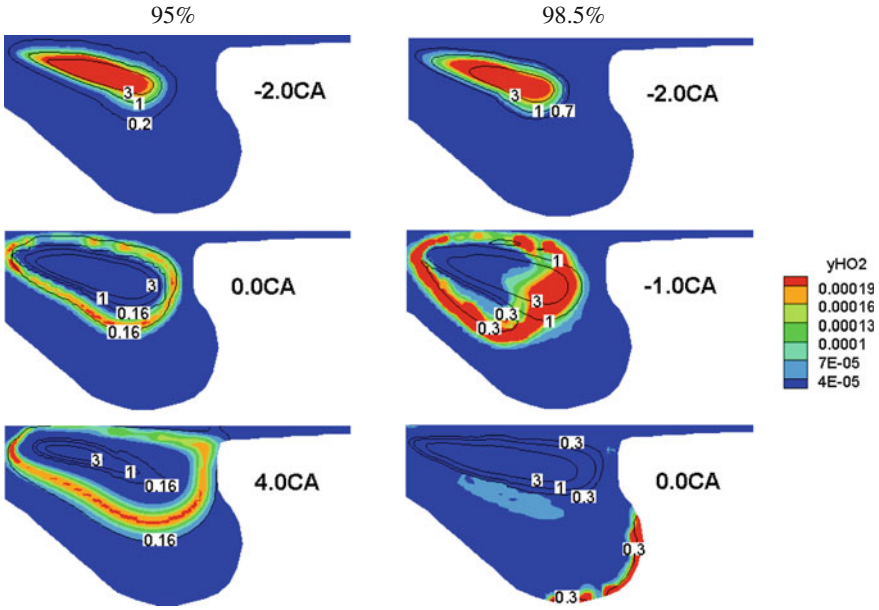

Fig. 19 HO_2 mass fraction contours at different crank angles for the 95 and 98.5 % syngas cases. Black lines indicate ϕ contour (ϕ = 0.16–3)

indicate significantly faster flame propagation for the 98.5 % syngas case compared to the 95 % syngas, since the gaseous equivalence ratios for the two cases are 0.7 and 0.17 (Table 3). In fact for the latter case, the flame gets extinguished at about 4° ATDC due to ultra lean conditions, and due to decreasing temperature and pressure during the expansion stroke. Furthermore, the comparison of HO_2 contours for the 97 % methane (Fig. 17) and 98.5 % syngas cases indicates significantly faster flame propagation in syngas-air mixture than that in methane-air mixture. However, as indicated in Table 3, the thermal efficiency is noticeably lower for 98.5 % syngas compared to that for 97 % methane. This is further discussed in the next section.

In summary, for certain operating conditions, the combustion process in syngas-based dual-fuel engine may become nearly spontaneous, which can possibly lead to knocking.

4.4 Dual-fuel Engine Performance and Emissions

Two of the performance parameters, i.e., IMEP and engine efficiency computed from pressure profiles (p-v diagram), are listed in Table 3 for all the five cases. At low load, the IMEP and engine efficiency are lower for the dual-fuel (90 % methane and 95 % syngas) cases compared to the single-fuel case, although they are slightly higher for syngas compared to those for methane. The loss of performance at low

load can be attributed to the incomplete combustion of gaseous fuel as discussed earlier. Thus, the use of gaseous fuels at low loads may adversely affect the engine performance and would require the optimization of other parameters, such as EGR and injection timing for the liquid fuel. In contrast, at high load (97 % methane and 98.5 % syngas), both methane and syngas are almost completely consumed through lean premixed combustion. Consequently for methane, the engine performance can be maintained or even enhanced with dual-fuel operation. However, for 98.5 % syngas, once the mixture is ignited, it is followed by nearly spontaneous combustion, with the result that the CA50 is −0.4° ATDC for this case. Consequently, the work output, IMEP, and engine efficiency are significantly reduced with syngas compared to those with methane and with single fuel (n-heptane).

The effect of gaseous fuel on dual-fuel engine emissions is summarized in Table 3, which lists the specific soot, NO_x, UHC, and CO emission values (mg/kwh) for the five cases at EVO (exhaust valve opening at 116° ATDC). Results indicate that with dual-fuel operation, the soot emission is significantly reduced at all loads, while the NO_x emission is increased. Moreover, the reduction in soot becomes more pronounced with syngas compared to that with methane at both low and high loads. In contrast, there is greater increase in NO_x emission with syngas than that with methane. The UHC emission is essentially eliminated with dual-fuel operation using syngas. However, the UHC and CO emission can significantly increase with methane at low load due to its incomplete combustion.

5 Summary and Conclusions

There is worldwide interest in developing renewable energy sources in a sustainable manner. Syngas and biogas offer significant potential in this context. These fuels can be produced from a variety of feedstock using different conversion methods and offer great flexibility with regard to their utilization in transportation and power generation systems. This chapter provides an overview of research dealing with the combustion and emissions of these fuels, both as stand-alone fuels or by blending with petroleum fuels. Conversion methods for producing these fuels from different biomass sources are also briefly reviewed.

There are notable differences between the combustion characteristics of these two fuels and those of hydrocarbon fuels. While the syngas composition can vary widely, it generally has lower heating value, lower density, higher mass diffusivity, higher flame speeds, and wider flammability limits. Its combustion leads to almost zero soot emission, although NO_x emission may be a concern depending upon its composition and operating temperatures. Similarly, biogas has lower heating value compared to hydrocarbon fuels, and its ignition and combustion characteristics can vary noticeably depending upon its composition. While there have been few studies focusing directly on biogas combustion, there is extensive literature on methane combustion, including ignition, extinction, flammability limits, flame speeds, cellular instabilities, and emissions. Results from many of these studies can be readily

used for analyzing the combustion and emission characteristics of biogas. For both syngas and biogas, a major challenge to combustion system designers is due to the wide variation in their composition. This also provides opportunities for fundamental and applied research on both the production and utilization aspects of such fuels. Fundamental combustion aspects requiring further research include cellular instabilities, flame stabilization and blowout behavior, turbulent flames, and emission characteristics. Such efforts would lead to the development of optimized systems for producing these fuels and provide guidelines for optimizing their composition for a given set of operating conditions.

The use of syngas and biogas in dual-fuel diesel engines has been a subject of numerous experimental and computational studies. In a dual-fuel operation, the gaseous fuel-air mixture is introduced through the intake valve, while the diesel fuel is injected and compression ignited. A general observation from these studies is that the engine performance and emission characteristics are significantly modified by the presence of gaseous fuel. For instance, the two-stage ignition process associated with the diesel fuel can be noticeably influenced depending upon the engine load and the relative amounts of gaseous and liquid fuels. The combustion characteristics are also significantly altered due to the presence of gaseous fuel. While the heat release in a diesel engine generally occurs through a hybrid combustion mode, involving rich premixed combustion and diffusion combustion, that in a dual-fuel engine also involves a lean combustion mode with a propagating flame. The dual-fuel operation at high-load conditions can provide significant reduction in soot and CO soot emissions, while maintaining the engine efficiency, provided the injection characteristics including the amount of pilot fuel can be optimized. However, the NO_x emission may increase, requiring a suitable strategy for lowering the temperatures. The dual-fuel strategy may be less effective at low load, resulting in lower thermal efficiency and higher UHC and CO emissions. Future work should be directed at optimizing the various parameters, such as injection timing, amount of pilot fuel injected, EGR, and multiple injections.

Acknowledgments Prof. Aggarwal's research over the years has been funded by several federal agencies, including NSF, NASA, AFOSR, EPA, Wright-Patterson Air Force Base, and ANL, as well as industry. His work concerning engine combustion and biomass-derived fuels has been supported by ANL. Many results in this monograph were computed by graduate students, Mr. Francesco Quesito and Mr. Xiao Fu.

References

Aggarwal SK (2009) Extinction of laminar partially premixed flames. Prog Energy Combust Sci 35:528–570

Aggarwal SK (2013) Simulations of combustion and emissions characteristics of biomass-derived fuels. In: Dahlquist E (ed) Technologies for converting biomass to useful energy: combustion, gasification, pyrolysis, torrefaction and fermentation. CRC Press, Boca Raton

Aggarwal SK, Awomolo O, Akber K (2011) Ignition characteristics of heptane-hydrogen and heptane-methane fuel blends at elevated pressures. Int J Hydrogen Energy 36:15392–15402

Azzoni R, Ratti S, Aggarwal SK, Puri IK (1999) The structure of triple flames stabilized on a slot burner. Combust Flame 119:23–40

Bauer CG, Forest TW (2001a) Effect of hydrogen addition on performance of methane-fueled vehicles. Part II: driving cycle simulation. Int J Hydrogen Energy 26:71–90

Bauer CG, Forest TW (2001b) Effect of hydrogen addition on the performance of methane-fueled vehicles. Part I: effect on SI engine performance. Int J Hydrogen Energy 26:55–70

Bika AS, Franklin L, Kittelson DB (2011) Engine knock and combustion characteristics of a spark ignition engine operating with varying hydrogen and carbon monoxide proportions. Int J Hydrogen Energy 36:5143–5152

Boehman A, Le Corre O (2008) Combustion of syngas in internal combustion engines. Combust Sci Technol 180:1193–1206

Bouvet N, Chauveau C, Gokalp I, Halter F (2011) Experimental studies of the fundamental flame speeds of syngas (H2/CO)/air mixtures. Proc Combust Inst 33:913–920

Bozzeli JW, Deam AM (1995) O + NNH: a possible new route for NO_x formation in flames. Int J Chem Kinet 27:1097–1109

Bridgwater AV (2012) Review of fast pyrolysis of biomass and product upgrading. Biomass Bioenergy 38:68–94

Briones AM, Som S, Aggarwal SK (2007) The effect of multi-stage combustion on NO_x emissions in methane-air flames. Combust Flame 149:448–462

Burbano HJ, Pareja J, Amell AA (2011) Laminar burning velocities and flame stability analysis of H_2/CO/air mixtures with dilution of N_2 and CO_2. Int J Hydrogen Energy 36:3232–3242

Burke M, Chaos M, Dryer F, Ju Y (2010) Negative pressure dependence of mass burning rates of H_2/CO/O_2/diluent flames at low flame temperatures. Combust Flame 157:618–631

Burke MP, Qin X, Ju Y (2007) Measurements of hydrogen syngas flame speeds at elevated pressures. In: 5th US combustion meeting

Caputo AC, Palumbo M, Pelagagge PM, Scacchia F (2005) Economics of biomass energy utilization in combustion and gasification plants: effects of logistic variables. Biomass Bioenergy 28:35–51

Chandra R, Vijay VK, Subbarao PMV, Khura TK (2011) Performance evaluation of a constant speed IC engine on CNG, methane enriched biogas and biogas. Appl Energy 88:3969–3977

Changwei J, Shuofeng W (2009) Effect of hydrogen addition on the idle performance of a spark ignited gasoline engine at stoichiometric condition. Int J Hydrogen Energy 34:3546–3553

Chatlatanagulchai W, Rhienprayoon S, Yaovaja K, Wannatong K (2010) Air/fuel ratio control in diesel-dual-fuel engine by varying throttle, EGR valve, and total fuel. SAE paper 2010-01-2200

Chatlatanagulchai W, Yaovaja K, Rhienprayoon S, Wannatong K (2010) Air–fuel ratio regulation with optimum throttle opening in diesel-dual-fuel engine. SAE paper 2010-01-1574

Cheng RK (2009) Synthesis gas combustion—fundamentals and applications. CRC Press, Boca Raton, pp 129–168

Chiang CH, Raju MS, Sirignano WA (1992) Numerical analysis of a convecting, vaporizing fuel droplet with variable properties. Int J Heat Mass Transf 35:1307

Cho HM, He BQ (2007) Spark ignition natural gas engines—a review. Energy Convers Manag 48:608–618

Ciatti S, Subramanian SN (2011) An experimental investigation of low-octane gasoline in diesel engines. J Eng Gas Turbines Power 133:092802-1–092802-11

Colantoni S, Gatta SD, Prosperis RD, Russo A, Fantozzi F, Desideri U (2010) Gas turbines fired with biomass pyrolysis syngas: analysis of the overheating of hot gas path components. J Eng Gas Turbines Power 132:061401–061408

(2008) Combust Sci Technol 180(6), May 2008

Curran HJ, Pitz WJ, Westbrook CK, Callahan CV, Dryer FL (1998) Oxidation of automotive primary reference fuels at elevated pressures. Proc Combust Inst 27:379–387

Czernik S, Bridgwater AV (2004) Overview of applications of biomass fast pyrolysis oil. Energy Fuels 18:590–598

Dam B, Love N, Choudhuri A (2011) Flashback propensity of syngas fuels. Fuel 90(2):618–625

Daniele SS, Jansohn P, Mantzaras J, Boulouchos K (2011) Turbulent flame speed for syngas at gas turbine relevant conditions. Proc Combust Inst 33:2937–2944

Das AK, Kumar K, Sung CJ (2011) Laminar flame speeds of moist syngas mixtures. Combust Flame 158:345–353

Das LM, Gulati R, Gupta PK (2000) A comparative evaluation of the performance characteristics of a spark ignition engine using hydrogen and compressed natural gas as alternative fuels. Int J Hydrogen Energy 25:783–793

Davis SG, Joshi AV, Wang H, Egolfopoulos F (2005) An optimized kinetic model of H_2/CO combustion. Proc Combust Inst 30:283–1292. http://ignis.usc.edu/Mechanisms/H2-CO/H2-CO.html

Dec JE (1997) A conceptual model of DI diesel combustion based on laser-sheet imaging. SAE paper 970873

Dimopoulos P, Bach C, Soltic P, Boulouchos K (2008) Hydrogen–natural gas blends fuelling passenger car engines: combustion, emissions and well-to-wheels assessment. Int J Hydrogen Energy 33:7224–7236

Ding N, Arora R, Norconk M, Lee SY (2011) Numerical investigation of diluent influence on flame extinction limits and emission characteristic of lean-premixed H_2–CO (syngas) flames. Int J Hydrogen Energy 36:3222–3231

Dryer FL, Chaos M (2008) Ignition of syngas/air and hydrogen/air mixtures at low temperatures and high pressures: experimental data interpretation and kinetic modeling implications. Combust Flame 152:293–299

Duc PM, Wattanavichien K (2007) Study on biogas premixed charge diesel dual fuelled engine. Energy Convers Manag 48:2286–2308

Fu X, Garner S, Aggarwal SK, Brezinsky K (2012) Numerical study of NO_x emissions from n-Heptane and 1-Heptene counterflow flames. Energy Fuel 26:879–888

Gauthier BM, Davidson DF, Hanson RK (2004) Shock tube determination of ignition delay times in full-blend and surrogate fuel mixtures. Combust Flame 139:300–311

Giles DE, Som S, Aggarwal SK (2006) NO_x emission characteristics of counterflow syngas diffusion flames with airstream dilution. Fuel 85:1729–1742

Gill SS, Tsolakis A, Dearn KD, Rodríguez-Fernández J (2011) Combustion characteristics and emissions of Fischer Tropsch diesel fuels in IC engines. Prog Energy Combust Sci 37:503–523

Golovichev V (n.d.) Mechanisms (combustion chemistry). (Online) Available at http://www.tfd.chalmers.se/~valeri/MECH.html. Accessed 2013

González FOC, Mahkamov K, Lora EES, Andrade RV, Jaen RL (2013) Prediction by mathematical modeling of the behavior of an internal combustion engine to be fed with gas from biomass, in comparison to the same engine fueled with gasoline or methane. Renew Energy 60:427–432

Gunaseelan VN (1997) Anaerobic digestion of biomass for methane production: a review. Biomass Bioenergy 13:83–114

Guo H, Smallwood GJ (2007) A numerical study on the effect of CO addition on extinction limits and NO_x formation in lean counterflow CH_4/air premixed flames. Combust Theory Model 11:741–753

Hall D, Rosillo-Calle F, Woods J (1991) Biomass, its importance in balancing CO_2 budgets. In: Grassi G, Collina A, Zibetta H (eds) Biomass for energy, industry and environment. In: 6th E. C. conference, Elsevier Science, London, pp 89–96

Hansen AC, Zhang Q, Lyne PWL (2005) Ethanol–diesel fuel blends—a review. Bioresour Technol 96:277–285

Huang J, Bushe WK, Hill PG, Munshi SR (2006) Shock initiated ignition in homogeneous methane–hydrogen–air mixtures at high pressure. Int J Chem Kinet 38:221–233

Hui X, Zhang, Z, Mu K, Wang Y, Xiao Y (2007) Effect of fuel dilution on the structure and pollutant emission of syngas diffusion flames. In: Proceedings of GT2007 ASME turbo expo: power for land, sea and air

Jain S, Li D, Aggarwal SK (2013) Effect of hydrogen and syngas addition on the ignition of iso-octane/air mixtures. Int J Hydrogen Energy 38:4163–4173

Kahraman N, Ceper B, Akansu SO, Aydin K (2009) Investigation of combustion characteristics and emissions in a spark-ignition engine fuelled with natural gas–hydrogen blends. Int J Hydrogen Energy 34(2):1026–1034

Kee RJ, Zhu H, Goodwin DG (2005) Solid-oxide fuel cells with hydrocarbon fuels. Proc Combust Inst 30:2379–2404

Kee RJ, Zhu H, Sukeshini AM, Jackson GS (2008) Solid oxide fuel cells: operating principles, current challenges, and the role of syngas. Combust Sci Technol 180:1207–1244

Kéromnès A, Metcalfe WK, Heufer KA, Donohoe N, Das AK, Sung CJ, Herzler J, Naumann C, Griebel P, Mathieu O, Krejci MC, Petersen EL, Pitz WJ, Curran HJ (2013) An experimental and detailed chemical kinetic modeling study of hydrogen and syngas mixture oxidation at elevated pressures. Combust Flame 160:995–1011

Kishore RV, Ravi MR, Ray A (2011) Adiabatic burning velocity and cellular flame characteristics of H2–CO–CO2–air mixtures. Combust Flame 158:2149–2164

Korakianitis T, Namasivayam AM, Crookes RJ (2011) Natural-gas fueled spark-ignition (SI) and compression-ignition (CI) engine performance and emissions. Prog Energy Combust Sci 37:89–112

Li J, Zhao Z, Kazakov A, Chaos M, Dryer FL, Scire JJ (2007) A comprehensive kinetic mechanism for CO, CH_2O, and CH_3OH combustion. Int J Chem Kinet 39:109–136

Lieuwen T, Mcdonell V, Santavicca D, Sattelmayer T (2008) Burner development and operability issues associated with steady flowing syngas fired combustors. Combust Sci Technol 180:1169–1192

Lieuwen TC, Yang V, Yetter RA (eds) (2009) Synthesis Gas combustion: fundamentals and applications. Taylor and Francis, London, 193–222

Lin Y, Tanaka S (2006) Ethanol fermentation from biomass resources: current state and prospects. Appl Microbiol Biotechnol 69:627–642

Linteris GT, Rumminger MD, Babushok VR (2008) Catalytic inhibition of laminar flames by transition metal compounds. Prog Energy Combust Sci 34:288–329

Liu J, Yang F, Wang H, Ouyang M, Hao S (2013) Effects of pilot fuel quantity on the emissions characteristics of a CNG/diesel dual fuel engine with optimized pilot injection timing. Appl Energy 110:201–206

Liu S, Zhou L, Wang Z, Ren J (2003) Combustion characteristics of compressed natural gas/diesel dual-fuel turbocharged compressed ignition engine. In: Proc Inst Mech Eng Part D: J Automobile Eng:217–833

Luessen HP (1997) Gas turbine technology for steel mill gas and syngas applications. ASME paper 97-GT-221

Ma F, Wang Y, Liu H, Li Y, Wang J, Zhao S (2007) Experimental study on thermal efficiency and emission characteristics of a lean burn hydrogen enriched natural gas engine. Int J Hydrogen Energy 32:5067–5075

McLean IC, Smith DB, Taylor SC (1994) The use of carbon monoxide/hydrogen burning velocities to examine the rate of the CO + OH reaction. Proc Combust Inst 25:749–757

Mittal G, Sung CJ, Yetter RA (2006) Autoignition of H_2/CO at elevated pressures in a rapid compression machine. Int J Chem Kinet 38:516–529

Mohan D, Pittman CU, Steele PH (2006) Pyrolysis of wood/biomass for bio-oil: a critical review. Energy Fuels 20:848–889

Monteiro E, Sotton J, Bellenoue M, Afonso Moreira N, Malheiro S (2011) Experimental study of syngas combustion at engine-like conditions in a rapid compression machine. Exp Thermal Fluid Sci 35:1473–1479

Morrone B, Andrea U (2009) Numerical investigation on the effects of natural gas and hydrogen blends on engine combustion. Int J Hydrogen Energy 34:4626–4634

Naber JD, Siebers DL, Di Julio SS, Westbrook CK (1994) Effects of natural gas composition on ignition delay under diesel conditions. Combust Flame 99:192–200

Natarajan J, Lieuwen T, Seitzman J (2007) Laminar flame speeds of H_2/CO mixtures: Effect of CO_2 dilution, preheat temperature, and pressure. Combust Flame 151:104–119

Natarajan J, Kochar Y, Lieuwen T, Seitzman J (2009) Pressure and preheat dependence of laminar flame speeds of $H_2/CO/CO_2/O_2$/He mixtures. Proc Combust Inst 32:1261–1268
Ollero P, Serrera A, Arjona R, Alcantarilla S (2003) The CO_2 gasification kinetics of olive residue. Biomass Bioenergy 24:151–161
Ouimette P, Seers P (2009) NO_x emission characteristics of partially premixed laminar flames of $H_2/CO/CO_2$ mixtures. Int J Hydrogen Energy 34:4626–4634
Park J, Hwang DJ, Kim KT, Lee SB, Kee SI (2004) Evaluation of chemical effects of added CO_2 according to flame location. Int J Energy Res 28:551–565
Patterson MA, Reitz RD (1998) Modeling the effects of fuel spray characteristics on diesel engine combustion and emission. SAE paper 1998-98-0131
Petersen EL, Kalitan DM, Barrett AB, Reehal SC, Mertens JD, Beerer DJ, Hack RL, McDonell VG (2007) New syngas/air ignition data at lower temperature and elevated pressure and comparison to current kinetics models. Combust Flame 149:244–247
Prathap C, Ray A, Ravi MR (2008) Investigation of nitrogen dilution effects on the laminar burning velocity and flame stability of syngas fuel at atmospheric condition. Combust Flame 155:145–160
Quattrocchi S (2014) Liftoff and blowout characteristics and structure analysis of syngas diffusion flames. MS thesis, Politecnico Di Torino
Quesito F, Santarelli M, Leone P, Aggarwal SK (2013) Biogas combustion in premixed flames or electrochemical oxidation in SOFC: exergy and emission comparison. J Energy Res Technol 135:021202-1–02120202120202120211
Ranzi E (2012) CRECK modeling—C1-C16 low and high temperature. (Online) Available at http://creckmodeling.chem.polimi.it/index.php/current-version-december-2012/c1c16-low-and-high-temperature. Accessed 2013
Rapagna S, Jand N, Kiennemann A, Foscolo PU (2000) Steam gasification of biomass in a fluidised-bed of olivine particles. Biomass Bioenergy 19:187–197
Richards KJ, Senecal PK, Pomraning E (2013) Converge (version 2.1.0). Convergent Science, Inc., Middleton
Rodrigues M, Walter A, Faaij A (2003) Co-firing of natural gas and biomass gas in biomass integrated gasification/combined cycle systems. Energy 28:1115–1131
Ryu K (2013) Effects of pilot injection timing on the combustion and emissions characteristics in a diesel engine using biodiesel–CNG dual fuel. Appl Energy 111:721–730
Sahoo BB, Sahoo N, Saha UK (2009) Effect of engine parameters and type of gaseous fuel on the performance of dual-fuel gas diesel engines—a critical review. Renew Sustain Energy Rev 13:1151–1184
Sahoo BB, Sahoo N, Saha UK (2012) Effect of H_2:CO ratio in syngas on the performance of a dual fuel diesel engine operation. Appl Therm Eng 49:139–146
San Diego (2002) The San Diego mechanism. (Online) Available at http://web.eng.ucsd.edu/mae/groups/combustion/mechanism.html
Senecal PK, Pomraning E, Richards KJ (2003) Multi-dimensional modeling of direct injection diesel spray liquid length and flame lift-off length using CFD and parallel detailed chemistry. SAE paper 2003-01-0243
Senecal PK, Richards KJ, Pomraning E, Yang T, Dai MZ, McDavid RM, Patterson MA, Hou S, Sethaji T (2007) A new parallel cut-cell Cartesian CFD code for rapid grid generation applied to in-cylinder diesel engine simulations. SAE paper 2007-01-0159
Shah A, Thipse S, Tyagi A, Rairikar S, Kavthekar K, Marathe N, Mandloi P (2011) Literature Review and Simulation of Dual Fuel Diesel-CNG Engines. SAE Paper 2011-26-0001
Shirk MG, McGuire TP, Neal GL, Haworth DC (2008) Investigation of a hydrogen-assisted combustion system for a light-duty diesel vehicle. Int J Hydrogen Energy 33:7237–7244
Singh S, Liang L, Kong SC, Reitz RD (2006) Development of a flame propagation model for dual-fuel partially premixed compression ignition engines. Int J Engine Res 7:65–75
Smith GP, Golden DM, Frenklach M, Moriarty NW, Eiteneer B, Goldenberg M, Bowman CT, Hanson RK, Song S, Gardiner WC, Lissianski VV, Qin Z, GRI Mech-3.0: http://www.me.berkeley.edu/gri_mech/

Som S, Aggarwal SK (2010) Effects of primary breakup modeling on spray and combustion characteristics of compression ignition engines. Combust Flame 157:1179–1193

Som S, Ramirez AI, Hagerdorn J, Saveliev A, Aggarwal SK (2008) A numerical and experimental study of counterflow syngas flames at different pressures. Fuel 87:319–334

Tao F, Reitz RD, Foster DE (2007) Revisit of diesel reference fuel (n-Heptane) mechanism applied to multidimensional diesel ignition and combustion simulations. In: Seventeenth international multidimensional engine modeling user's group meeting at the SAE congress, 15 Apr 2007, Detroit, Michigan

Tijmensen MJA, Faaij APC, Hamelinck CN, van Hardeveld MRM (2002) Exploration of the possibilities for production of Fischer Tropsch liquids and power via biomass gasification. Biomass Bioenergy 23:129–152

Tomita E, Harada Y, Kawahara N, Sakane A (2009) Effect of EGR on combustion and exhaust emissions in supercharged dual-fuel natural gas engine ignited with diesel fuel. SAE paper 2009-01-1832

Vagelopoulos CM, Egolfopoulos FN (1998) Direct experimental determination of laminar flame speeds. Proc Combust Inst 27:513–519

Venkateswaran P, Marshall A, Shin DH, Noble D, Seitzman J, Lieuwen T (2011) Measurements and analysis of turbulent consumption speeds of H_2/CO mixtures. Combust Flame 158:1602–1614

Walton SM, He X, Zigler BT, Wooldridge MS (2007) An experimental investigation of the ignition properties of hydrogen and carbon monoxide mixtures for syngas turbine applications. Proc Combust Inst 31:3147–3154

Wang H, You X, Joshi AV, Davis SG, Laskin A, Egolfopoulos F, Law CK (2007) USC Mech version II. High-temperature combustion reaction model of H_2/CO/C1-C4 compounds. http://ignis.usc.edu/USC_Mech_II.htm, May 2007

Wang J, Chen H, Liu B, Huang Z (2008a) Study of cycle-by-cycle variations of a spark ignition engine fueled with natural gas–hydrogen blends. Int J Hydrogen Energy 33:4876–4883

Wang L, Weller CL, Jones DD, Hanna MA (2008b) Contemporary issues in thermal gasification of biomass and its application to electricity and fuel production. Biomass Bioenergy 32:573–581

Watanabe M, Inomata H, Arai K (2002) Catalytic hydrogen generation from biomass (glucose and cellulose) with ZrO_2 in supercritical water. Biomass Bioenergy 22:405–410

Werther J, Saenger M, Hartge EU, Ogada T, Siagi Z (2000) Combustion of agricultural residues. Prog Energy Combust Sci 26:1–27

Wikipedia (2014) Biogas. (Online) Available at http://en.wikipedia.org/wiki/Biogas. Accessed 2014

Yan B, Wu Y, Liu C, Yu JF, Li B, Li ZS (2001) Experimental and modeling study of laminar burning velocity of biomass derived gases/air mixtures. Int J Hydrogen Energy 36:3677–3769